Gravity-driven differences in fluvial sediment transport fluxes on Mars and Earth

Lisanne Braat (lisanne.braat@esa.int, @LisanneBraat)[1,2], Muriel Z. M. Brückner[3], Elliot Sefton-Nash[1], and Michael P. Lamb[2]

[1]European Space Agency (ESA), Noordwijk, The Netherlands
[2]California Institute of Technology (Caltech), Pasadena CA, United States of America
[3]University of Exeter, Exeter, United Kingdom

April 5, 2023

Abstract

Studies of fluvial landforms on the surface of Mars have become more detailed since rover data became available (e.g. water-deposited sediment in Gale crater by Curiosity and the Jezero delta by Perseverance). As surface interpretations become more detailed, we need to pay more attention to differences between Earth and Mars to fully describe the processes that determine fluvial geomorphology on Mars. In this study, we isolate and clarify the effect of gravity on fluvial sediment transport with an analytical model of a transport capacity limited alluvial channel. We use and compare 32 predictors to calculate the sediment transport rate for a range of grain sizes (clay to boulders) and a lognormal sediment distribution. The results indicate that 1) bigger grains are mobilised on Mars and transported in suspension. 2) The magnitude of the suspended transport flux is larger on Mars and therefore the total flux as well. Consequently, the gravity effect on transport rates varies with grain size, with the biggest effect on the bed load-suspended load transition. We expect that these gravity-driven differences in fluvial sediment transport create differences in sediment sorting, morphology and stratigraphy between Earth and Mars. We advise to avoid total load predictors in the future for surfaces besides Earth, because the effect of gravity varies by transport mode. Additionally, our results stress the significance of gravity on hydraulic and sedimentary processes and provide new insights into Earth-derived fluvial sediment transport predictors for estimating transport rates and morphological change on Mars and other planets and moons.

1 Introduction

Similar to geomorphic activity on Earth, surface dynamics on Mars shape the Martian landscape. Since the first Viking images in 1976, many geomorphic features at the surface of Mars have been identified from orbit that indicate fluvial activity in the past Carr (2012), such as depositional channels (Fig. 1A-C; e.g. Dickson et al., 2021), deltas (Fig. 1C-G; e.g. Di Achille & Hynek, 2010; Hauber et al., 2013; S. A. Wilson et al., 2021; De Toffoli et al., 2021), alluvial fans (Fig. 1H; e.g. Moore & Howard, 2005; Kraal et al., 2008; S. A. Wilson et al., 2021), valleys and valley networks (Fig. 1I; e.g. Hynek & Phillips, 2003; Hynek et al., 2010; Bahia et al., 2022), open (or chain) crater lakes (Fig. 1J; e.g. Cabrol & Grin, 1999, 2001, 2003; Fassett & Head III, 2008) and outflow channels (Fig. 1K-L; e.g. Sharp, 1973; Baker & Milton, 1974; Harrison & Grimm, 2008). Ground observations from the Curiosity, Opportunity and Perseverance rovers have supported these interpretations (e.g. Grotzinger et al., 2015; Mangold et al., 2021). These geomorphic features formed as a result of entrainment, transport and settling of sediments in a Newtonian fluid, most likely liquid water. If indeed water created these fluvial landforms, they can help us infer knowledge about past hydrological conditions on Mars, volumes of erosion and deposition and about timescales of their formation, provided that sediment transport rates can be estimated Komar (1979); Kleinhans (2005); Grotzinger et al. (2013). In addition to the derivation of past environmental and climate conditions, they can also help determine the potential for and the preservation of past life. However, fluvial sediment transport on Mars is difficult to estimate since sediment transport fluxes (volume/time, i.e., transport rates) depend strongly on sediment grain size, transport mode and hydrodynamic conditions, all parameters that need to be estimated as of lack of available data. We can systematically investigate those parameters by applying the physical and empirical transport equations derived for Earth under Martian conditions.

Fluvial sediment transport on Earth has been studied since the early 20^{th} century and is typically divided into three modes Bagnold (1966); Francis (1973): Bed load, suspended load and wash load. Bed load is the portion of the grains that is transported close to the bed by rolling, sliding and saltation. Smaller grains are picked up by turbulence and are transported higher in the water column as suspended sediment. Wash load are the smallest grain sizes that are sufficiently fine that they are transported uniformly through the water column as a result of extremely low settling velocities. Processes of sediment entrainment, transport and settling are likely the same on Earth and Mars. However, differences in sediment transport fluxes are expected because of Mars-specific parameters, such as lower gravity and different sediment densities (resulting from different geology). Previous studies estimated discharge and fluvial sediment fluxes from channel dimensions based on basic hydraulic relations (e.g. Komar, 1979; Kleinhans et al., 2010; Salese et al., 2020; Amy & Dorrell, 2021). Although those studies give a good approximation on flow characteristics and associated sediment transport volumes, we still lack a systematic understanding of how the sediment fluxes differ between the two planets and how this affects morphology and stratigraphy on Mars.

Gravity, especially, affects the potential for sediment transport because gravity drives transport of water and sediment on a given slope and controls the settling velocity of the sediment. On the one hand, the shear stress acting on the riverbed induces entertainment, which depends linearly on water depth, slope, and gravity, suggesting that transport rates reduce under lower Martian gravity as compared to transport on Earth. On the other hand, reduced settling forces on the sediment grains might counteract this trend, leading to larger transport rates for the same flow. In order to address this problem, past research has investigated the effect of gravity on the initiation of motion and suspension Komar (1980); Burr et al. (2006); Grotzinger et al. (2013). Those studies found that bigger grains are comparatively more easily picked up by flow on Mars. Based on their results, they suggest that fluvial sediment transport is more efficient and that hyper-concentrated flows might be common. However, they did not calculate sediment transport fluxes.

For Earth, several fluvial sediment transport predictors have been developed to predict transport rates, depending on the near-bed sediment concentrations, shear stress induced by the flow and the sediment properties. In this study we considered 20 bed load transport equations. These empirical equations are often based on the difference between the non-dimensional shear stress induced by the flow and the critical shear stress for the initiation of motion of the sediment with some fitting coefficients: $\phi_b = A(\theta - \theta_{cr})^B$. Though some variation exists, depending on the predictor, this difference is raised to a power of a coefficient B larger than 1 and multiplied by a coefficient A, making the correlations highly dependent on sediment type, mixture and experimental setup. Some exceptions exist that only use the non-dimensional shear stress, but not the critical shear stress. Suspended transport depends on a reference concentration and reference height with which a rouse profile is calculated and integrated: $\phi_s = \int_a^h E_s(\frac{h-z}{z}\frac{a}{h-a})^R dz$. The reference concentration is typically a function of the non-dimensional shear stress or movability number, which is the ratio of the shear velocity and settling velocity. We considered 11 predictors for suspended transport.

As visible from the many coefficients in the equations, fluvial sediment transport equations are semi-empirical equations that are fitted to physical experiments or field data. These experiments were conducted under Earth gravity conditions and likely differ from Martian conditions. However, it is practically impossible to conduct physical experiments under reduced gravity conditions for long enough time periods to represent realistic sediment transport rates. In addition, more physical reliable models using the discrete element method (DEM) using computational fluid mechanics (CDF) (e.g. Schmeeckle, 2014), in which the movement of individual grains are modelled, are extremely computational expensive. Consequently, analytical and numerical models can help to test existing transport laws and provide estimates of transport rates on other planets. Although there is a risk that gravity components might be hidden in some of the coefficients, past experiments testing different sediment densities in combination with non-dimensional analysis have helped addressing potential biases Kleinhans (2005).

In order to provide a practical framework to estimate actual fluvial sediment transport rates for field sites on Mars, we model absolute sediment transport rates in comparison to Earth. We isolate and clarify the effect of gravity on fluvial sediment transport by means of an analytical model. Our study has three aims: 1) testing the response of hydraulic and associated sediment transport parameters for a range of gravity; 2) estimating total sediment flux for a range of sediment grain sizes and a mixed sediment distribution; 3) testing the suitability of a range of sediment transport predictors for application on Mars. This will allow us to directly compare sediment transport between Earth and Mars. Only when we understand the effects of gravity on sediment erosion and deposition, we can confidently apply and adapt knowledge of fluvial geomorphology on Earth to the surface of Mars, i.e., use Earth analogues.

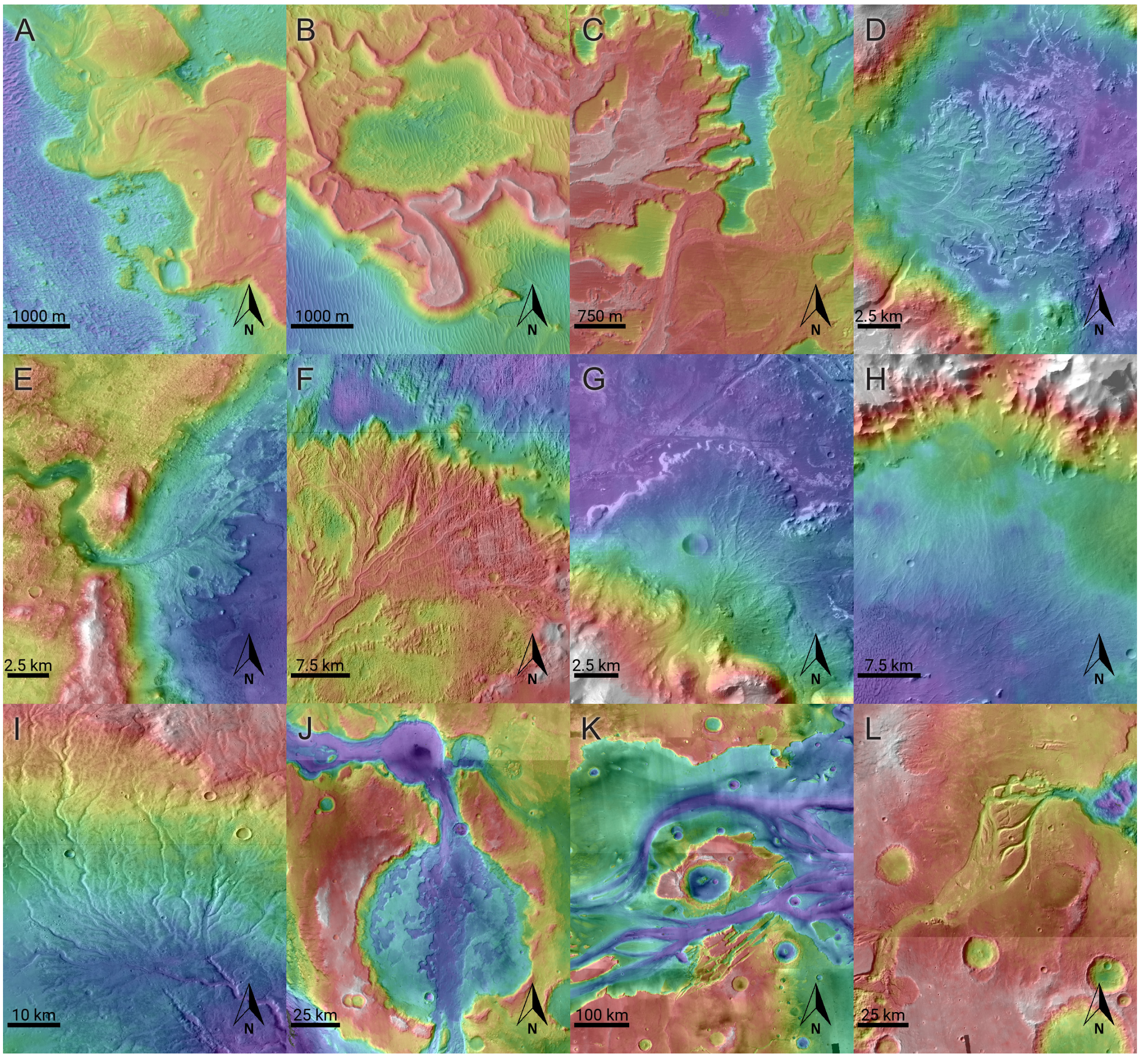

Figure 1: Examples of fluvial landforms on Mars. Inverted meandering depositional channel at (A-B) Aeolis Dorsa (HiRISE, 5.8°S, 205.4°W and 5.0°S, 205.1°W) and (C) Eberswalde (HiRISE, 23.8°S, 33.6°W). Deltas at (D) Eberswalde (MOLA/HRSC+CTX, 23.8°S, 33.6°W), (E) Jezero crater (CTX, 18.5°N, 282.7°W), (F) Aeolis Dorsa (MOLA/HRSC+CTX, 6.2°S, 208.6°W) and (G) Holden crater (MOLA/HRSC+CTX, 26.9°S, 34.5°W). (H) Alluvial fans (MOLA/HRSC+CTX, 21.4°S, 39.4°W), (I) valley drainage network (MOLA/HRSC+CTX, 42.1°S, 92.8°W), (J) chain lake system (MOLA/HRSC+CTX, 3.0°N, 16.1°W), (K) mega-outburst channels (MOLA/HRSC+CTX, 27°N, 58°W) and (L) outburst channel (MOLA/HRSC+CTX, 15.5°S, 38.6°W).

Table 1: Model boundary conditions

Boundary conditions flow				
Width	W	200	m	
Slope	S	0.001	m/m	Fig. 6d uses a range: 0.0001–0.01 m/m
Water density	ρ	1000	kg/m^3	
Temperature	T	4	$°C$	
Discharge	Q	2000	m^3/s	Fig. 3 and 6c use a range: 500–15000 m^3/s
Gravity acceleration	g	3.7, 9.8	m/s^2	Fig. 3 and 6a use a range: 1–12 m/s^2
Boundary conditions sediment				
Sediment density	ρ_s	29	kg/m^3	
Grain size	D	1μ–1	m	
Nikuradse roughness length	k_s	0.03	m	
Calculated parameters				
Relative density	R	1.8	–	
Kinematic viscosity	ν	1.54e-6	m^2/s	

2 Methods

We isolate the effects of gravity on fluvial sediment transport with a model parameterised in MATLAB R2021b that calculates hydraulic and sediment transport parameters for a variety of grain sizes and sediment transport predictors. The model describes fluvial sediment transport in a channel with a fixed bed, where transport is not limited by sediment availability, but transport capacity limited. We use an idealised analytical model with which we look at relative changes between model scenarios. Most importantly, a scenario with Earth gravity is compared with a Mars gravity scenario. This approach allows us to better understand the role of gravity on transport predictors of open-channel, transport capacity limited flows and allows us to isolate effects of Martian conditions on total fluvial sediment transport fluxes for a wide range of sediment grain sizes.

2.1 Model input

We use constant channel dimensions with a fixed channel width and slope (Table 1) that could be easily obtained from orbital data. In addition, we choose an arbitrary temperature to calculate viscosity and water density (Table 1). To calculate flow, one more boundary condition is required. The most obvious parameter would either be water discharge or water depth. Keeping one or the other equal between model scenarios will lead to different outcomes. Though both were investigated, we will use discharge as a boundary condition and the results for a water level boundary will be shown in the Supplement. For gravity on Mars we use a value of 3.7 m/s^2 and 9.8 m/s^2 for Earth. Throughout the paper results using gravity on Mars are denoted with red and on Earth with blue.

For sediment boundary conditions we use a sediment density of 2900 kg/m^3, which is in the density range of basalt (as in Burr et al., 2006; Amy & Dorrell, 2021). This igneous rock type is more common on Mars than on Earth and has a higher density than quartz 2650 kg/m^3 which is typically used for Earth. The grain size range used varies from clay to large boulders. Transport is calculated for all grain sizes individually (uniform mixtures) and for one lognormal sediment distribution (Figure 2).

2.2 Hydraulic calculations

Equations 1–4 are used to derive hydraulic parameters. From discharge Q in m^3/s, slope S in m/m and width W in m the hydraulic radius R_w in m, Chézy roughness C in $m^{0.5}/s$, velocity u in m/s and water depth h in m are calculated iteratively. The hydraulic radius (Equation 1) is based on the geometry of the channel. The geometry of the channel is assumed to be rectangular with similar wall and bed roughness. The White-Colebrook function (Equation 2) is a drag law and assumes hydraulic rough flow. The Chézy equation (Equation 3) is a conservation of momentum equation and assumed 1-D unidirectional, steady uniform flow. Equation 4 is conservation of mass and assumes incompressible flow.

$$R_w = \frac{hW}{2h + W} \tag{1}$$

$$C = 5.75\sqrt{g}\log\left(\frac{12h}{k_s}\right) \tag{2}$$

$$u = C\sqrt{R_w S} \tag{3}$$

$$h = \frac{Q}{Wu} \tag{4}$$

where g is gravity in m/s^2 and k_s is the Nikuradse roughness length in m.

Based on hydraulic radius, the bed shear stress τ in N/m^2 (Equation 5) is calculated. Many authors replace the hydraulic radius with water depth to simplify the equations (Equations 3 and 5). This is generally a good approximation because rivers are much wider than they are deep.

$$\tau = \rho g R_w S = \rho u_*^2 \tag{5}$$

where ρ is the water density in kg/m^3 and u_* is the shear velocity in m/s.

In addition to the hydrodynamic parameters, we calculated the Froude and the Reynolds number to investigate the effects of gravity on the transition between subcritical and supercritical and laminar and turbulent flow, respectively. These transitions determine the degree of mixing and the direction of momentum in the water column which determine the capacity for water and sediment transport towards the downstream.

$$Fr = \frac{u}{\sqrt{gh}} \tag{6}$$

$$Re = \frac{uh}{\nu} \tag{7}$$

where ν is the kinematic viscosity in m^2/s.

2.3 Fluvial sediment transport calculations

The velocity with which particles settle from the water column results from balancing the drag with the gravitational forces. We use the equation from Ferguson & Church (2004) because this equation is a physics-based, simple, universal equation for all grain sizes (Eq. 8).

$$w_s = \frac{RgD^2}{C_1\nu + \sqrt{0.75C_2RgD^3}} \tag{8}$$

where w_s is the settling velocity in m/s, D is the grain size in m, R is the relative density and C_1 and C_2 are constants. C_1 is the constant in Stokes' equation for laminar settling and C_2 is the constant drag coefficient. Both coefficients are related to the smoothness/roughness, angularity and sphericity of the particles, here 20 and 1, respectively. The angularity of particles on Mars is expected to be higher due to shorter transport distances, however, this effect is expected to be minimal for alluvial rivers Schumm & Stevens (1973).

The mobility of the bed can be expressed by the particle mobility parameter, i.e. Shields number (Equation 9). The Shields number θ is a nondimensionalisation of the shear stress. The initiation of motion of particles on the bed is commonly described by the Shields curve, which provides a critical Shields number θ_{cr} for the initiation of motion of each grain size. Over the years, many critical Shields curves have been formulated Mantz (1977); Brownlie (1981); Collins & Rigler (1982); Komar & Clemens (1986); Soulsby (1997); Paphitis (2001); Zanke (2003); Cao et al. (2006); Rijn (2007); Beheshti & Ataie-Ashtiani (2008); Simões (2014); Kleinhans et al. (2017); Lapôtre & Ielpi (2020). Some of these equations have also been used in the past for Mars and Titan Kleinhans (2005); Burr et al. (2006); Lamb et al. (2012); Amy & Dorrell (2021). Here we use Zanke (2003) (Equation 10), a physics-based equation, whereas most other equations are empirical fits to flume data and not valid for all grain sizes. A more detailed comparison of all the equations can be found in the Supplement (Fig.9).

$$\theta = \frac{\tau}{(\rho_s - \rho) g D_{50}} \tag{9}$$

$$\theta_{cr} = \frac{(1-n) tan(\phi/1.5) K}{(1 + 1.8 \frac{u'_{rms,b}}{u_b}^2) * (1 + 0.4 (1.8 \frac{u'_{rms,b}}{u_*})^2 tan(\phi/1.5) K)} \tag{10}$$

where ϕ is the angle of repose, n the porosity fraction, K is a parameter for the cohesive effect. On how to calculate the different velocity components, we refer to the original paper of Zanke (2003). The critical Shields curve from Zanke (2003) needs to be calculated iteratively to gain a single curve independent of flow conditions.

As mentioned, fluvial sediment transport is divided into three transport modes: Bed load, suspended load and wash load. In practice the transition between the modes is gradual, and therefore visually subjective and difficult to define. Bagnold (1966) defines the transition between bed load and suspension by the ratio of the downward component (settling velocity) and the upward component (turbulence) called the movability number k, which leads to the following ratio: $w_s/u_* = k$. Various values for k have been used in the past ([1–1.79] see Komar, 1980), however in this research we use the traditional value of $k = 1$ assuming no sediment interactions.

Additional parameters that were calculated are the particles Reynolds number Re_p, the Bonnefile parameter D_*, i.e., non-dimensional grain size, and the advection length A (Eq. 11–13). The advection length provides the average horizontal distance travelled by a particle before settling.

$$Re_p = \frac{D_{50}^{1.5} \sqrt{Rg}}{\nu} \tag{11}$$

$$D_* = D_{50} \left(\frac{Rg}{\nu^2} \right)^{1/3} \tag{12}$$

$$A = \frac{uh}{w_s} \tag{13}$$

Since wash load is typically not limited by transport capacity but by sediment availability, it is very difficult to determine for Mars. We are ignoring wash load in our analysis but will come back to it in the discussion.

2.4 Fluvial sediment transport equations

Many different equations exist to determine bed load and suspended sediment transport. In our analysis we tested 20 bed load transport equations, 11 suspended transport equations and 1 total load equation (Table 2.4). In our analysis of total sediment transport fluxes per grain size, we only combined and compared bed load and suspended load equations of the same authors Einstein (1950); Engelund & Fredsoe (1976); Rijn (1984a,b); de Leeuw et al. (2020). A discussion on which equations were believed more and less reliable can be found in the Supplement.

2.5 Total sediment flux

We calculated the total fluvial sediment flux based on a hypothetical sediment mixture (Figure 2). The sediment composition is a lognormal distribution with the peak between the medium and coarse sand class (Figure 2b). The distribution includes sediment fractions from clay ($\geq 1\ \mu m$) to boulders ($\leq 630\ mm$). A sediment flux was calculated for every sediment class based on the median grain size of that class using Einstein (1950). We multiplied this flux with the fraction of the total sediment composition of that class (Fig. 2b). The summation of the fluxes of these classes provides the total sediment flux.

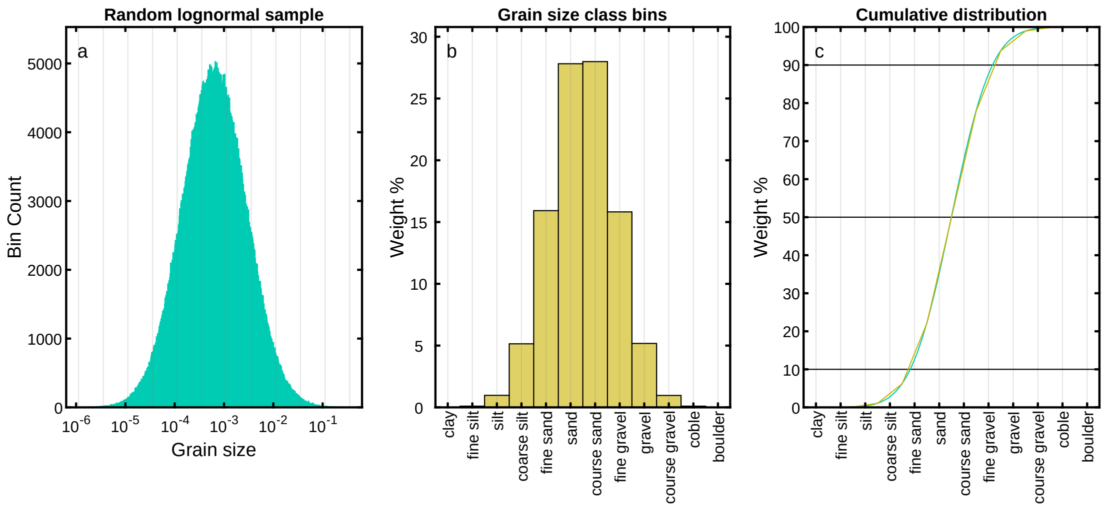

Figure 2: Grain size mixture created from a lognormal grain size distribution (a), divided into grain size classes (b) and visualised as a cumulative distribution (c).

3 Results

3.1 Effects of gravity on hydrodynamics

The results show that gravity has clear effects on the flow parameters. For a given range of discharges, water depth is inversely correlated with gravity, leading to increasing water depth and hydraulic radius on Mars as compared to Earth (Fig. 3). The net effect of increased water depth and reduced gravity results in a higher roughness (lower C). In turn, lower gravity reduces velocity, bed shear stress and shear velocity. The hydraulic parameters are increasingly sensitive to changes in

Bed load transport predictors		
Reference	Einstein predictor Φ_b	Comments
Einstein (1942) as in Carrillo et al. (2021)	$2.1exp^{\frac{-0.391}{\theta}}$	
Meyer-Peter & Müller (1948)	$8(\theta-\theta_{cr})^{1.5}$	0.047 was replaced by θ_{cr}
Meyer-Peter & Müller (1949) as in Carrillo et al. (2021)	$(4\theta-0.188)^{1.5}$	
Einstein (1950) as in de Leeuw et al. (2020)	$3.97(\theta-\theta_{cr})^{1.5}$	
Bagnold (1966) as in Kleinhans (2005)	$\frac{e_b u \tau}{(\rho_s-\rho) g \cos S(\tan\phi-\tan S)}/(\sqrt{gRD_{50}^3})$	$e_b = a\log 3.28u+b$ where a and b depend on grain size
K. C. Wilson (1966) as in Soulsby & Damgaard (2005)	$12\theta^{1.5}$	
Ashida & Michiue (1972) as in Carrillo et al. (2021)	$17(\theta-\theta_{cr})(\sqrt{\theta}-\sqrt{\theta_{cr}})$	0.05 was replaced by θ_{cr}
Luque & van Beek (1976)	$5.7(\theta-\theta_{cr})^{1.5}$	
Engelund & Fredsoe (1976)	$5p(\sqrt{\theta}-0.7\sqrt{\theta_{cr}})$	$p=(1+(\frac{\frac{\pi}{6}\beta}{\theta-\theta_{cr}})^4)^{-0.25}$, $\beta=1$ as in Garcia (1991)
Parker (1979) as in Kleinhans (2005); Carrillo et al. (2021)	$11.2\frac{(\theta-\theta_{cr})^{4.5}}{\theta^3}$	0.03 was replaced by θ_{cr}
Smart (1984)	$4.2S^{0.6}(\frac{u}{u_*})\sqrt{\theta}(\theta-\theta_{cr})$	
Rijn (1984a)	$0.053D_*^{-0.3}T_0^{2.1}$	$T_0=\frac{u_*^2-u_{*cr}^2}{u_{*cr}^2}$
Rijn (1984a) as in Kleinhans (2005)	$0.1D_*^{-0.3}S_0^{1.5}$	$S_0=\frac{\theta-\theta_{cr}}{\theta_{cr}}$
Nielsen (1992)	$12\sqrt{\theta}(\theta-\theta_{cr})$	
Ribberink (1998)	$11(\theta-\theta_{cr})^{1.65}$	
Hunziker & Jaeggi (2002)	$5(\theta-\theta_{cr})^{1.5}$	0.05 was replaced by θ_{cr}
Cheng (2002)	$13\theta^{1.5}exp(-\frac{\theta_{cr}}{\theta^{1.5}})$	0.05 was replaced by θ_{cr}
Camenen & Larson (2005)	$12\theta^{1.5}exp(-4.5\frac{\theta_{cr}}{\theta})$	
Wong & Parker (2006)	$4.93(\theta-\theta_{cr})^{1.6}$	0.047 was replaced by θ_{cr}
Wong & Parker (2006)	$3.97(\theta-\theta_{cr})^{1.5}$	0.0495 was replaced by θ_{cr}
Suspended transport predictors		
Reference	Reference concentration / Entrainment E_s	Comments
Einstein (1950)	$\frac{1}{32.2}\frac{\Phi_b}{\sqrt{\theta}}$	
Engelund & Fredsoe (1976)	$\frac{0.65}{(1+\lambda^{-1})^3}$	$\lambda=\sqrt{\frac{\theta-\theta_{cr}-(\frac{\pi}{6}\beta p)}{(0.027(R+1)\theta)}}$, $\beta=1$
Smith & McLean (1977)	$\frac{0.65*\gamma S_0}{1+\gamma S_0}$	$S_0=\frac{\theta-\theta_{cr}}{\theta_{cr}}$, $\gamma=0.0024$ as in de Leeuw et al. (2020)
Itakura & Kishi (1980) as in Garcia (1991)	$0.008(\frac{0.14u_*\Omega}{w_s\theta}-1)$	$\Omega=\frac{\theta}{0.143}(2+\frac{exp(-A^2)}{\int_A^\infty exp(-z^2)dz})-1$, $A=\frac{0.143}{\theta}-2$
Celik & Rodi (1984) as in Garcia (1991)	$1.13\frac{C_m}{\int_{0.05}^1((\frac{1-z}{z})(\frac{0.05}{1-0.05}))^R dz}$	$C_m=0.034(1-\frac{k_s}{h}^{0.06})\frac{u_*^2 u}{gRhw_s}$
Rijn (1984b)	$0.015\frac{DS_0^{1.5}}{aD_*^{0.3}}$	
Akiyama (1986) as in Garcia (1991)	$3*10^{-12}Z^{10}(1-\frac{5}{Z})$	$Z=\frac{u_*}{w_s}Re_p^{0.5}$
Garcia (1991)	$\frac{1.3*10^{-7}Z^5}{1+\frac{1.3*10^{-7}}{0.3}Z^5}$	$Z=\frac{u_*}{w_s}Re_p^{0.6}$
McLean (1992)	$\frac{0.065\gamma S_0}{1+\gamma S_0}$	$S_0=\frac{\theta-\theta_{cr}}{\theta_{cr}}$, $\gamma=0.004$
Wright et al. (2004)	$\frac{7.8*10^{-7}Z^5}{1+\frac{7.8*10^{-7}}{0.3}Z^5}$	$Z=\frac{u_*}{w_s}Re_p^{0.6}$
de Leeuw et al. (2020)	$4.74*10^{-4}\frac{u_*}{w_s}^{1.77}Fr^{1.18}$	
Total transport predictor		
Reference	Einstein predictor Φ_t	Comments
Engelund & Hansen (1967)	$\frac{0.05u^5}{\sqrt{g}C^3R^2D}$	

Table 2: List of bed, suspended, and total load fluvial sediment transport predictors. We indicate where it was not possible to obtain the predictor directly from the original paper due to the age of the paper, language barriers or pay walls.

gravity for decreasing gravities. Gravity has no effect on the Reynolds number, meaning that the transition from laminar to turbulent flow is independent of gravity for a given discharge. The effect of gravity on the Froude number is existent, but negligible. All scenarios considered were subcritical.

The effects of gravity are different when water depth is used as independent variable (boundary condition) instead of discharge (Fig. 8). Since water depth is in this case constant, Chézy roughness, velocity, shear stress, and shear velocity are strongly affected by a change in gravity. The relation between gravity and shear stress is now linear (Fig. 8f) because there is no gravity component in the water depth, as compared to Fig. 3f. The Reynolds number becomes dependent on gravity and Froude number and hydraulic radius are no longer dependent on gravity (Fig. 8b and d). The graphs related to these calculations are included in the Supplement, however the rest of the results presented are based on discharge as independent variable.

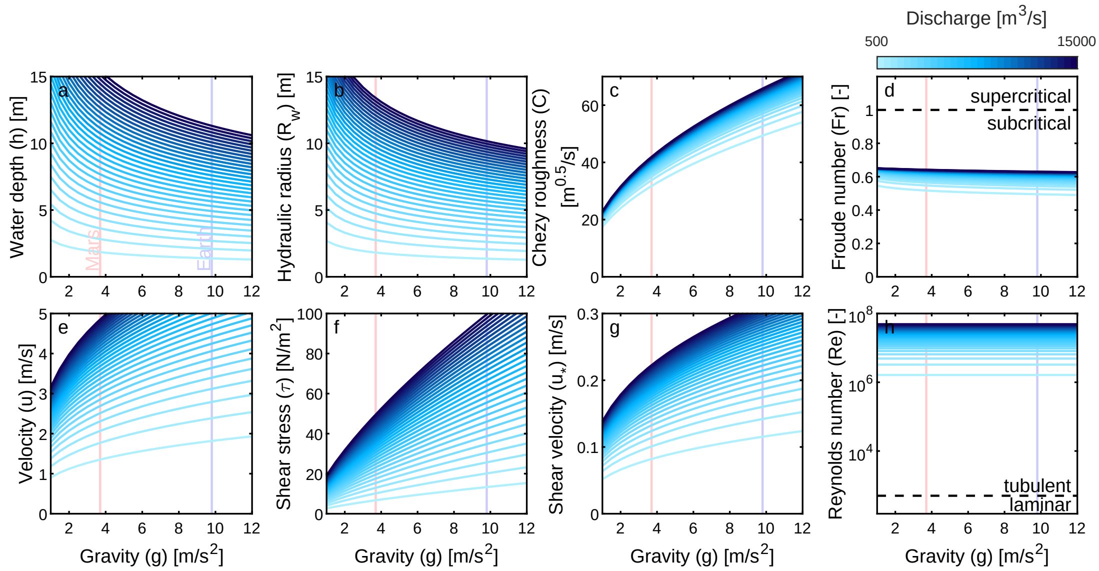

Figure 3: Hydrodynamic variables (a) water depth h $[m]$, (b) hydraulic radius R_w $[m]$, (c) Chézy roughness C $[m^{0.5}/s]$, (d) Froude number Fr $[-]$, (e) velocity u $[m/s]$, (f) shear stress τ $[N/m^2]$, (g) shear velocity u_* $[m/s]$, and (h) Reynolds number Re $[-]$ as a function of gravity g $[m/s^2]$ for a range of discharges Q $[m^3/s]$. All y-axis variables are dependent variables calculated from independent variables discharge, slope and width.

3.2 Effects of gravity on fluvial sediment transport fluxes

The response of the flow parameters to changes in gravity in turn affect the transport flux of the sediment. We test the response of a range of grain sizes under a fixed water discharge of 2000 m^3/s to better understand the effects of Martian gravity on sediment transport as compared to Earth (Figure 4). Despite the fact that lower gravity on Mars reduces shear stress and shear velocity, which would decrease fluvial sediment transport rates, the mobility of the sediment increases as a result of two additional mechanisms: Firstly, settling velocity is lower under lower gravity (Figure 4a), resulting in a reduced tendency of the sediment to deposit, as noted by previous studies. This effect is independent of the initial boundary conditions (i.e., water depth or discharge; Figure 10a), and depends only on gravity, grain size and relative density. The reduced settling velocity, despite lower Martian velocities, increases the transport distance of the grains, as expressed by the advection length (Figure 4d). Secondly, Martian gravity results in higher Shields and movability numbers (Figure 4b and c) similar to previous findings by Komar (1980); Burr et al. (2006); Grotzinger et al. (2013), increasing the tendency of the sediment to be entrained and suspended. As a result, larger grains can be picked up and transported in suspension for Martian gravity.

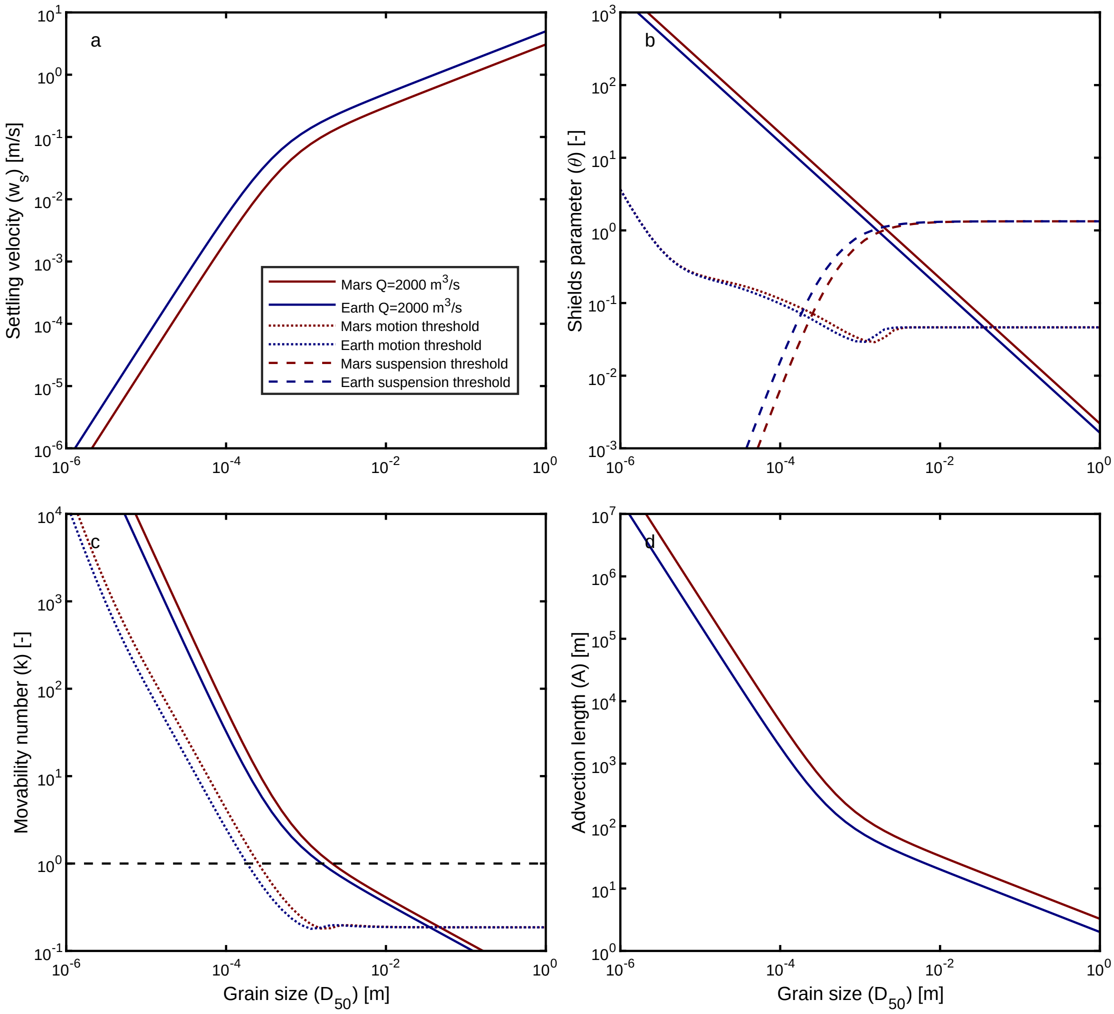

Figure 4: Fluvial sediment transport parameters (a) settling velocity w_s $[m/s]$, (b) Shields parameter θ $[-]$, (c) movability number k $[-]$, (d) advection length A $[m]$ as a function of grain size D_50 $[m]$ for Mars (red) and Earth (blue) gravitational acceleration g $[m/s^2]$ and a given discharge Q $[m^3/s]$. Please note the logarithmic scale in all subplots.

To better understand the effects of gravity on the different modes of transport, we show grain size dependent transport for various transport predictors (Fig. 5 from Table. 2.4). Despite the order of magnitude differences in predicted transport rates between different predictors, almost all equations agree on the relative effect of gravity. The influence of gravity on bed load transport is limited, except for the largest grains that on Earth lie below the threshold of motion. This bed load transport flux difference is caused by the higher non-dimensional shear stress on Mars that results in picking up larger grains for the same discharge (Fig. 4b).

The influence of gravity on suspended transport is much stronger than for bed load transport (Fig. 5b). Lower gravity results in more suspended sediment transport. This gravity difference for suspension translates to the total transport per grain size (Fig. 5c). Because suspended sediment is more important for smaller grain sizes, absolute and relative (Fig. 5d), the effect of gravity is stronger for smaller grain sizes (Fig. 5c).

The grain size class at the bed load-suspension transition is affected strongest, leading to a peak of about 5 times higher transport rates for Mars (Fig. 5e). This is because for this grain size, there is predominantly suspended transport on Mars, whereas bed load transport on Earth. Which sediment class is affected most depends on the flow conditions that define the bed-suspension load transition, which in our scenarios is sand.

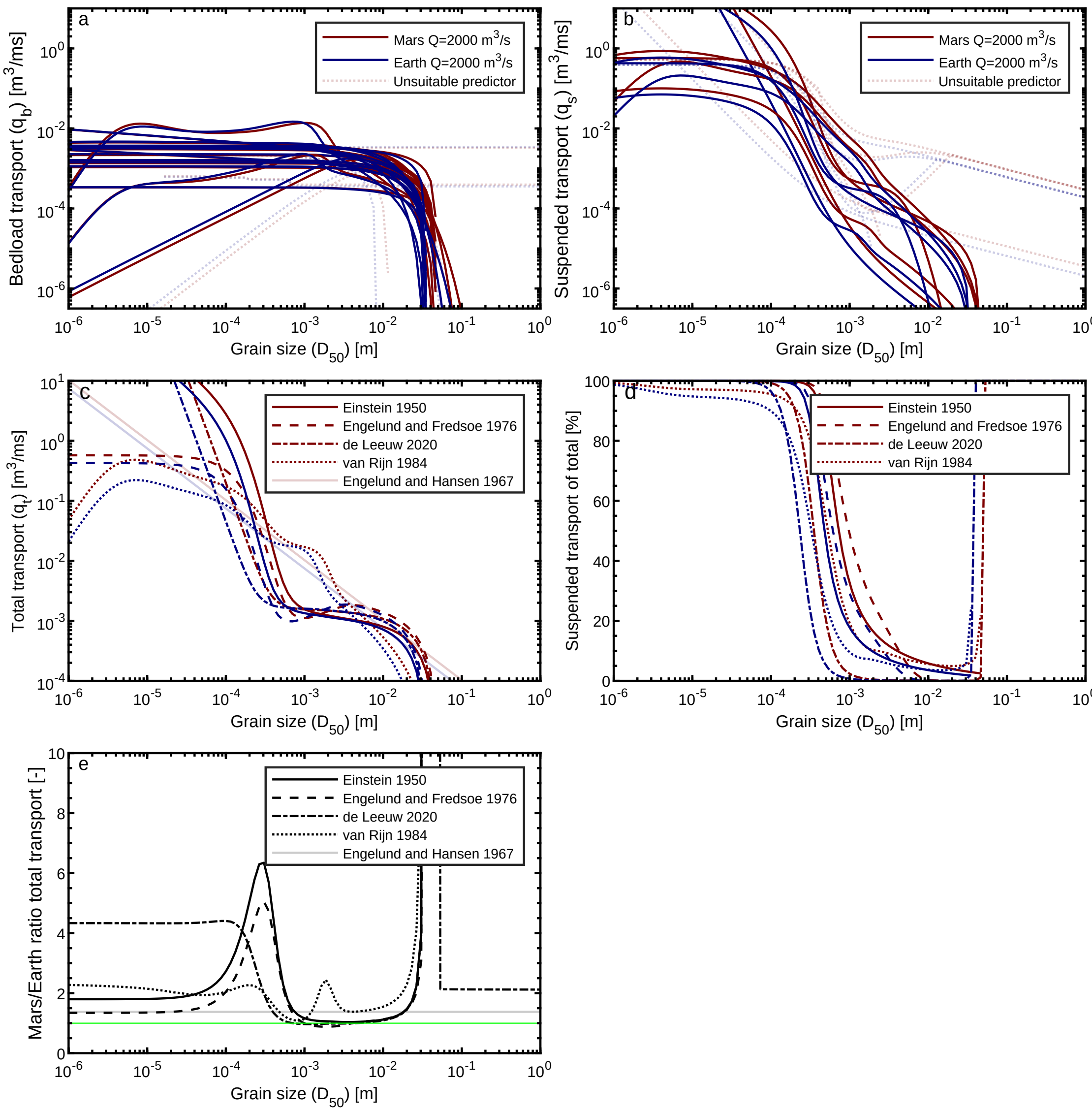

Figure 5: Fluvial transport rates as a function of grain size. (a) Bed load transport q_b $[m^3/ms]$, (b) suspended transport q_s $[m^3/ms]$, (c) total transport q_t $[m^3/ms]$, (d) percentage of suspended transport of the total transport [%], (e) total transport ratio of Mars and Earth $[-]$ for Mars (red) and Earth (blue) gravity acceleration g $[m/s^2]$ and a given discharge Q $[m^3/s]$.

3.3 fluvial sediment transport flux for a given sediment mixture

Instead of calculating fluvial sediment transport for a uniform, single grain size, the sediment transport flux can also be calculated for a sediment mixture (Fig. 2), which is more realistic for natural rivers. For a lognormal sediment distribution, the total sediment transport rate increases exponentially with decreasing gravity (Fig. 6a). The contribution of different grain size classes varies slightly between Earth and Mars: On Mars there is a relatively larger contribution of larger grains (Fig. 6b).

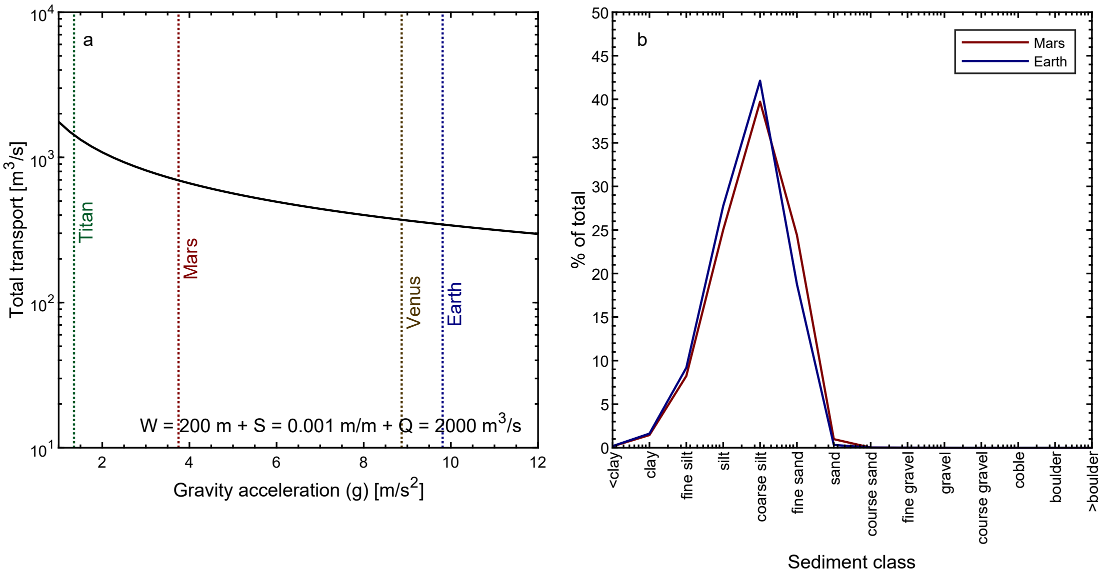

Figure 6: Total fluvial transport rates for the lognormal grain size distribution (Fig. 2) using Einstein (1950). Each grain size is summed up relative to their fraction of the total load. (a) Total sediment transport flux q_t $[m^3/ms]$ for a range of gravity g $[m/s^2]$, (b) contribution of each sediment fraction to the total transport flux.

4 Discussion

4.1 Fluvial sediment transport fluxes on Mars

The fluvial sediment transport fluxes on Mars differ from Earth for a couple of reasons. Firstly, the initiation of motion is affected by gravity. Bigger grains are picked up from the bed due to a higher Shields parameter for a given discharge. So consequently, a smaller discharge is needed on Mars compared to Earth to move sediment and therefore increase transport, non-linearly, after initiation of motion. In addition, bigger grains are transported in suspension because of the same principle. Secondly, there is relatively more transport in suspension because the larger Shields parameter shifts the transition zone for bed-suspended load transport towards bigger grain size classes. In absolute terms there is also more suspension due to steepening of the non-linear relationship between increasing transport rates and decreasing gravity. This further reduces the ratio between bed load and suspended transport.

Without calculating sediment fluxes, Komar (1980); Burr et al. (2006) already showed that Martian flows could have transported bigger grain sizes in different transport modes. The authors related this to the differences in settling velocity and stream-flow velocity. In addition, Amy & Dorrell (2021) identified that suspended sediment flows have a slightly higher potential for transport on Mars. We find similar results from our computations of sediment transport fluxes, and quantify how the relative distribution of sediment between transport modes differs by calculating bed load and suspended load transport rates separately and as a total flux.

Total fluvial sediment transport rates are higher on Mars than on Earth for the same water discharge, sediment distribution and geometry. This is due to a combination of the previously mentioned effects, but mainly because of the larger amount of suspended transport. Larger sediment fluxes are calculated for each grain size, but especially for fine particles. Consequently, sediment fractions experience gravity differently because of the transport mode, so this changes the distribution of grain size fractions. Finer particles are affected more by gravity, because they are more commonly transported as suspension. Also, for sediment mixtures the transport on Mars is higher for a given discharge.

Lastly, not only the entrainment is affected, but also sediment settling. Lower gravity reduces settling velocities and advection length on Mars. Settling velocity depends on particle size and therefore creates vertical sorting when grains settle in a standing body of water, and longitudinal sorting in decelerating currents Ferguson & Church (2004).

4.2 Implications for geomorphology

Because gravity affects fine and coarse sediment fractions differently, we expect differences in geomorphology due to different ratios of sediment fractions and disparities in sediment sorting. The change in ratio between bed load and suspended transport has implications for a variety of geomorphological features across scales. Bed load transport is thought to affect in-channel morphological development through deposition and erosion that affect bed form dynamics and height, point bar and in-channel bar formation and growth. Bed load fractions as the 'channel-building' fractions therefore alter lateral behaviour of rivers, such as migration rates or number of channels through bar and island formation. The suspended fraction on the other hand determines channel-floodplain interactions when high flows lead to distribution of sediments onto the floodplain. Levee formation, crevasse splays and cut-off infilling affect channel migration and floodplain elevation.

Previous studies suggested that high suspended loads in sand-bed rivers promote vertical bar accretion and subsequent conversion to floodplain Nicholas (2013). As a result, an increase in relative suspended transport fractions might reduce bedform and bar migration and instead redistribute sediments onto the floodplain. This in turn drives the formation of narrower, sinuous channels and reduce channel branching Nicholas (2013). As a result of the absolute increase in suspended sediment, we expect a higher likelihood of the formation of overbank deposits during channel flooding on Mars than on Earth with faster and more prominent levee formation. It would be difficult to find evidence for this on Mars in the present day because the fine overbank deposits would have been easily eroded Hayden et al. (2019).

Another consequence of higher relative and absolute suspension rates is an increased chance of hyper-concentrated flows Burr et al. (2006); Komar (1980), especially if fine (weathered) sediment was abundantly present. Flows on Mars likely carry more sediment and is therefore possibly more erosive (an idea also suggested by Bagnold (1962)). When entering a standing water body, these flows can create stratification or density-driven flows due to density differences, resulting in a higher likelihood of turbidity currents and deposits on Mars.

Additionally, we expect lower depositional slopes, mainly due to the settling of particles over a longer distance (longer advection length due to reduced settling velocities). This will transport more sediment to the delta front and the prodelta van der Vegt et al. (2016). In addition, this may impact the slopes of delta foresets and therefore also stratigraphy, which is important to realise when preparing missions aiming to drill for sediment samples in the search for biosignatures Vago et al. (2017). This is in contrast to Konsoer et al. (2018), who state that suspended dominated flows on Mars require steeper slopes all other things being equal. They argue that lower gravity acceleration requires steeper slopes to produce the same bed shear stress and move sediment. This is true for Martian turbidity currents, however the grains also weigh less and for alluvial channels this combined effect results in more sediment transport and settling over larger distances, which would result in lower depositional slopes. In addition we expect that larger suspended sediment fractions in deltas lead to deeper channels, less reworking, and a rugose delta brink contour, both with and without cohesivity van der Vegt et al. (2016).

Lastly, the most obvious effect of gravity on geomorphology is caused by the total transport rate. This research has shown that depositional landforms can develop faster on Mars for the same discharge. The fluvial sediment transport rate could be up to 6 times faster for the conditions tested here. Consequently, fluvial depositional landforms visible on Mars would have required a shorter period of fluvial activity to form compared to Earth. Or in other words, in the same amount of time, the same discharge would develop a much larger landform on Mars. Yet, the temporal variability of fluvial sediment transport is large. It has been argued that the intermittency factor, defined as the fraction of total time in which bankfull flow would accomplish the same amount of sediment transport as the real hydrograph, is much smaller on Mars Hayden et al. (2019). This would result is longer fluvial activity for landforms on Mars despite transport being more efficient. Nonetheless, further research on the intermittency factors on Mars is necessary as estimated intermittency factors for Mars could reflect the duration of no activity periods rather than the amount of sediment transport during active periods Hayden et al. (2019).

4.3 Missing effects and uncertainties

In this research we attempt to isolate the effect of gravity on transport and geomorphology. However, there are more processes that should be considered on Mars to make a completely fair comparison. For example, there are expected effects of ice on sediment transport. Mars used to be more accommodating for fluid water in the Noachian and Early Hesperian, but most likely it has always been cold Fairén (2010); Wordsworth (2016). Ice and permafrost largely reduce the mobility of channels and enhance overbank deposition Piliouras et al. (2021), which would further enhance the effect we expect by enhanced suspended sediment transport. Additionally, we assume that sediment transport is limited by the capacity of the flow to carry sediment and we therefore assume unlimited availability of sediment to accommodate unhindered entrainment. However this not only unlikely due to possible permafrost, but also due to geological constrains like bed armouring Ferdowsi et al. (2017), cohesive sediment Braat et al. (2017); Ledden et al. (2004); Peakall et al. (2007); Edmonds & Slingerland (2010) and bedrock layers Lamb et al. (2015).

Wash load is a mode of transport that is typically not limited by transport capacity, but by sediment availability and is therefore not calculated in this study. We acknowledge that wash load, even though it is impossible to determine, was likely more significant on Mars under lower gravity but otherwise similar circumstances as Earth Burr et al. (2006); Komar (1980). Due to the lower settling velocities, a larger portion of the sediments would contribute to the wash load instead of to the suspended load. It should be noted however, that the total transport rate of wash load is not limited by flow, but by supply. So even though short duration of hyper-concentrated flows are possible due to high wash or suspended loads, it is not likely they were sustained for a long period of time because high supply rates of fines for a long time are unlikely.

A gravity effect that could potentially be important for geomorphology that was not accounted for in this study in the effect of gravity on the angle of repose. In fluvial sediment transport predictors of the form $A(theta - theta_{cr})^B$, the coefficient A is dependent on the friction angle, i.e. angle of repose Soulsby & Damgaard (2005); Kleinhans et al. (2011). According to Kleinhans et al. (2011) the static angle of repose increases with 5^circ with reduced gravity (10%), but the dynamic angle of repose decreased with 10^circ leading to larger avalanche sizes. Because of these contrasting results, this is difficult to incorporate their results in this study.

4.4 Best practice for planetary fluvial sediment transport calculations

Firstly, we recommend to use a separate bed load and suspended load predictor. By using a total load predictor, important effects of gravity on sediment transport are overlooked. Figure 5c and e include the total load equation from Engelund & Hansen (1967), with which all grain sizes are effected uniformly by gravity (Figure 5e), leading to a poorly estimated fluvial sediment transport flux. First, they do not account for a strong increase in transport for the grains sizes that pass the threshold from bed load to suspended load for lower gravity. Second, the suspended load should increase relatively to the bed load transport in total and for all grain sizes for lower gravity. Third, the predictor of Engelund & Hansen (1967) does not account for a critical shear stress, a non-negligible factor. The predictor of Engelund & Hansen (1967) is a popular equation in terrestrial fluvial geomorphology because it is simple and predicts the correct order of magnitude of sediment transport. It is a popular equation in 2D horizontal models because it creates excellent channel patterns Baar et al. (2019). However, since our results have shown that gravity acts differently on suspended sediment compared to bed load transport, total load equations that are calibrated for Earth should be avoided in case of Mars.

Secondly, we recommend to use a bed load predictor that includes a critical value for mobility. Some predictors are more useful than others as many predictors are developed with a single purpose in mind, for example just for coarse-grained rivers. Also, very few studies investigated combined bed load and suspended load transport (e.g. Einstein, 1950; Engelund & Fredsoe, 1976; Rijn, 1984a,b; de Leeuw et al., 2020). Because the thresholds for motion and suspension differ on Mars, we prefer equations that contain a critical value for mobility Meyer-Peter & Müller (1948); Einstein (1950); Ashida & Michiue (1972); Luque & van Beek (1976); Engelund & Fredsoe (1976); Parker (1979); Smart (1984); Rijn (1984a); Nielsen (1992); Ribberink (1998); Hunziker & Jaeggi (2002); Cheng (2002); Camenen & Larson (2005); Wong & Parker (2006). Predictors that are therefore not recommended for Mars are Einstein (1942); Meyer-Peter & Müller (1949); Bagnold (1966); K. C. Wilson (1966) and are plotted transparently in Figure 5a. It should be noted that while Camenen & Larson (2005); Cheng (2002) use a critical value, these predictors do not cut off the transport at large grain sizes but use an exponential reduction in transport related to the critical Shield's parameter. Meyer-Peter & Müller (1949) does not use a realistic critical shields value, but does have a cut off. A few predictors unexpectedly decrease in bed load transport for smaller grain sizes Einstein (1942); Engelund & Fredsoe (1976); Rijn (1984a). This is slightly counter intuitive. Regardless of whether this is correct or not, this is unimportant as the suspended transport component of these grain sizes quickly becomes several magnitudes larger. A few equations deviate from the majority without specific reason Rijn (1984a); Smart (1984), it is unclear how reliable these predictors are. Many of the bed load predictors that consistent, predictable, and therefore reliable results are mostly of the form $A(\theta - \theta_{cr})^B$, many modelled after Meyer-Peter & Müller (1948).

Suspended load predictors show more variation than bed load predictors. The predictor from Itakura & Kishi (1980) is not valid for all grain sizes and is therefore not useful for this purpose. In addition, the predictors from Celik & Rodi (1984); Akiyama (1986); Garcia (1991); Wright et al. (2004) show transport rates that are too high for large grain sizes, because the values are higher than all bed load transport predictors and pass the no motion threshold. These equations are also deemed unreliable for this purpose (see Figure 5b). The predictor by de Leeuw et al. (2020) increases transport exponentially for small grain sizes. Theoretically this might me correct in an idealised situation, though in practice this is unpractical

(Figure 6b). Mud and especially clay particles should have lower sediment transport rates because erosion is typically not unhindered, due to for example cohesion. This equation was not marked as unreliable for this purpose, but this should be considered when interpreting results including fine sediments.

Considering all predictors discussed, though more reliable options are available, we recommend the combination of the bed load and suspended load predictor of Einstein (1950) as these equations were developed by the same author, they are simple, widely used and tested, are valid for all grain sizes and do not show relations that cannot be explained logically.

Finally, we stress to clearly describe your independent variables, i.e. boundary conditions. When calculating sediment transport on Mars, channel size and slope can be obtained from terrain models, however, one independent hydrodynamic variable is always required in addition. As shown in the Supplement, a water level boundary can lead to completely different conclusions on the fluvial sediment transport comparison between Earth and Mars compared to results with a discharge boundary. Aside from discharge and water level, one could also input velocity or bed shear stress as their independent variable (Figure 7). Though transport on Mars is always higher, different boundary conditions lead to different conclusions (Figure 7). The choice of boundary conditions will depend on the data availability and the research question.

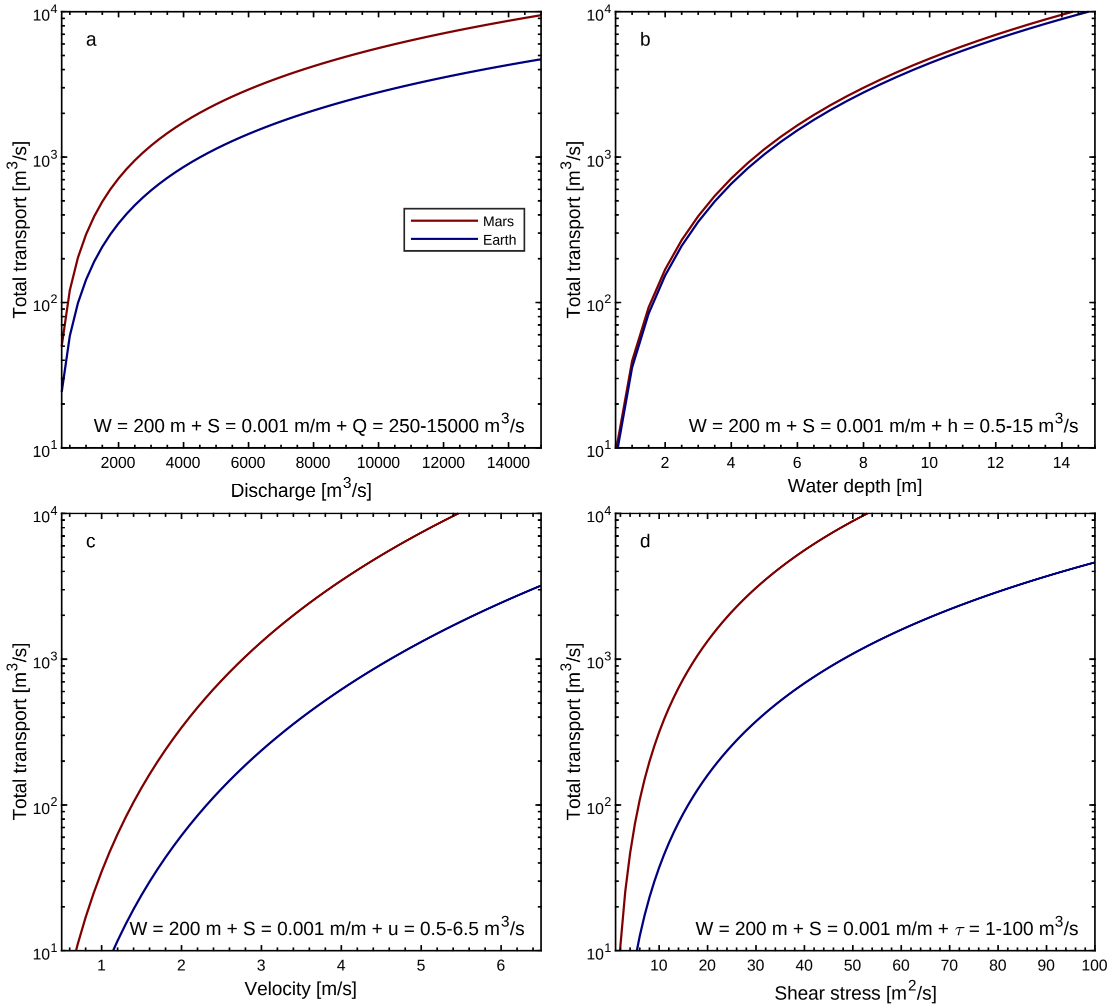

Figure 7: Total fluvial transport rates for different independent variables (i.e. boundary conditions, i.e. input conditions) related to flow. Total sediment transport flux q_t $[m^3/ms]$ for a range of (a) discharges Q $[m^3/s]$ (original settings), (b) flow depths h $[m]$ (Supplement), (c) velocities u $[m/s]$, (d) shear stresses τ $[m^2/s]$. All transport rates are based on Einstein (1950) and the sediment mixture (Fig. 2).

4.5 Application to other planets and moons

The focus of this research has been on defining differences in fluvial sediment transport between Earth and Mars. However, these results can also be valuable to calculate sediment transport on other planetary bodies or moons with significant surface liquid (Figure 6a). The calculations can be adapted to any liquid Newtonian flow at the surface. Titan is an obvious target, as Titan has a hydrocarbon cycle in which liquid methane and ethane flow like a liquid at the surface. Images from the imaging Subsystem (ISS) Porco et al. (2004) and Visual and Infrared Mapping Spectrometer (VIMS) Brown et al. (2004) aboard the Cassini-Huygens mission have shown erosional and depositional landforms Nixon et al. (2018) including alluvial fans Birch et al. (2016), active river deltas Wall et al. (2010), and river valleys (e.g. Burr et al., 2013). The gravity effect for Titan can be obtained from this study (Figure 3 and 6a), however, there is also a significant effect of sediment and fluid density that adds to transport differences that are not considered here. Previous authors Witek & Czechowski (2015); Burr et al. (2006) already showed that transport, and especially suspended transport, in rivers on Titan is more effective than in terrestrial rivers for the same discharge, similar to results we observed for Mars. Potential future work is to analyse combined density and gravity effects on fluvial sediment transport with our parameterised model with the aim to interpret data from Titan.

Channels have also been identified on Venus that could be attributed to ancient fluvial activity Khawja et al. (2020). Resolution of surface features at decametre scales on Venus shall be enabled by VenSAR (a phased array synthetic aperture radar) Ghail et al. (2018) aboard ESA's EnVision mission, currently scheduled for launch in 2031. EnVision, and future missions observing the Venutian surface will provide data to which the approach of this paper could be applied.

A Supplement

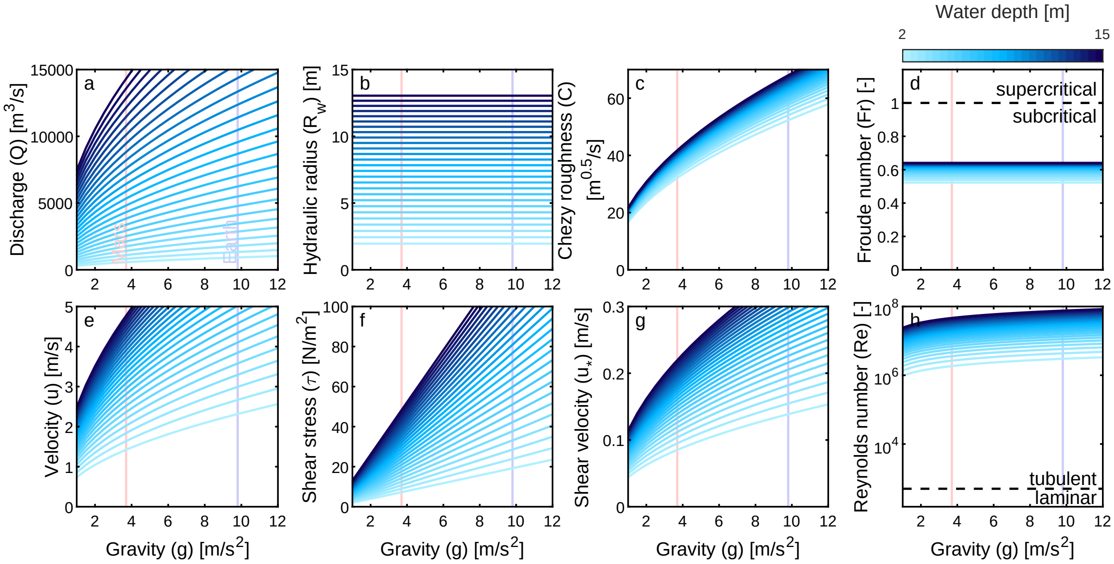

Figure 8: Hydrodynamic variables (a) water discharge Q $[m^3/s]$, (b) hydraulic radius R_w $[m]$, (c) Chézy roughness C $[m^{0.5}/s]$, (d) Froude number Fr $[-]$, (e) velocity u $[m/s]$, (f) shear stress τ $[N/m^2]$, (g) shear velocity u_* $[m/s]$, and (h) Reynolds number Re $[-]$ as a function of gravity g $[m/s^2]$ for a range of water depths h $[m]$.

A.1 Thresholds for the initiation of motion

In this study we considered 18 equations for the initiation of motion of 16 publications (Table 3). In Fig. 9 we plotted the traditional equations of Brownlie (1981); Soulsby (1997) and added less common equations of Mantz (1977) as described in Komar & Clemens (1986) and Paphitis (2001) and their own equations. From Paphitis (2001) we plotted three different equations and from Komar & Clemens (1986) we used their more generalised form of Collins & Rigler (1982). Because this equation was most reliable, we did not use any of the other equations mentioned in Komar & Clemens (1986) or Collins & Rigler (1982). The Soulsby (1997) equation is sometimes also cited as Soulsby & Whitehouse (1997) and is for example used in Kleinhans et al. (2017); Lapôtre & Ielpi (2020). Additionally, we plotted more modern equations of the initiation of motion from Zanke (2003); Cao et al. (2006); Rijn (2007); Simões (2014).

In addition to the equation in the plot we also considered the Zanke (2003) fit from Kleinhans (2005), but was discarded because of the limited grain size range compared to the original Zanke (2003). We discovered that citation of Brownlie (1981) in Miedema (2010); Righetti & Lucarelli (2007) seemed incorrectly cited. The equation differed from the original and the dimensional critical shear stress seemed to increase incorrectly for smaller grain sizes. A similar trend was observed with the equation from Beheshti & Ataie-Ashtiani (2008) and was therefore discarded.

Table 3: Curves for the initiation of motion

Critical Shields curves		
Mantz (1977) as in Komar & Clemens (1986); Paphitis (2001)	$\theta_{cr} = 0.1 Re_*^{-0.3}$	Fig. 9
Brownlie (1981)	$\theta_{cr} = 0.22 Re_p^{-0.6} + 0.06 * 10^{-7.7 Re_p^{-0.6}}$	Fig. 9
Brownlie (1981) as in Miedema (2010); Righetti & Lucarelli (2007)	$\theta_{cr} = 0.22 Re_p^{-0.9} + 0.06 exp(-17.77 * Re_p^{-0.9})$	discarded
Soulsby (1997) / Soulsby & Whitehouse (1997)	$\theta_{cr} = \frac{0.3}{1+1.2D_*} + 0.055(1 - exp(-0.02D_*))$	Fig. 9
Soulsby (1997) / Soulsby & Whitehouse (1997) as in Kleinhans et al. (2017)	$\theta_{cr} = 0.5(\frac{0.3}{1+1.2D_*} + 0.055(1 - exp(-0.02D_*)))$	discarded
Paphitis (2001)	$\theta_{cr} = \frac{0.188}{1+Re_*} + 0.0475(1 - 0.699 exp(-0.015 * Re_*))$	Fig. 9
Paphitis (2001)	$\theta_{cr} = \frac{0.273}{1+1.2D_*} + 0.046(1 - 0.576 exp(-0.02 * D_*))$	Fig. 9
Zanke (2003)	$\theta_{cr} = \frac{(1-n)*tan(\frac{\phi}{1.5})*K}{(1+1.8\frac{u'_{rms,b}}{u_b})^2*(1+0.4(1.8\frac{u'_{rms,b}}{u_*})^2*tan(\frac{\phi}{1.5})*K)}$	Main paper; Fig. 9
Zanke (2003) fit from Kleinhans (2005)	$\theta_{cr} = 0.145 Re_p^{-0.33} + 0.045 * 10^{-1100 Re_p^{-1.5}}$	discarded
Cao et al. (2006)	$Re_p < 6.61 \Rightarrow \theta_{cr} = 0.1414 Re_p^{-0.2306}$ $6.61 \leq Re_p \leq 282.84 \Rightarrow$ $\theta_{cr} = (1 + (0.0223 Re_p)^{2.8358})^{\frac{0.3542}{3.0946 Re_p^{0.6769}}}$ $Re_p > 282.84 \Rightarrow \theta_{cr} = 0.045$	Fig. 9
Rijn (2007)	$D_* < 4 \Rightarrow \theta_{cr} = 0.115 D_*^{-0.5}$ $4 \leq D_* < 10 \Rightarrow \theta_{cr} = 0.14 D_*^{-0.64}$	Fig. 9
Critical movability curves		
Komar & Clemens (1986)	$k_{cr} = 1.8 Re_*^{-1.3}$	discarded
Komar & Clemens (1986)	$k_{cr} = 1.14 Re_*^{-1.37}$	discarded
Komar & Clemens (1986)	$k_{cr} = 5.54 Re_p^{-1.09}$	discarded
Beheshti & Ataie-Ashtiani (2008)	$0.4 < D_* \leq 10 \Rightarrow k_{cr} = 9.6674 D_*^{-1.57}$ $10 < D_* < 500 \Rightarrow k_{cr} = 0.4738 D_*^{-0.226}$	discarded
Simões (2014)	$k_{cr} = 0.215 + \frac{6.79}{D_*^{1.7}} - (0.075 exp(-2.62 * 10^{-3 D_*}))$	Fig. 9
Critical shear stress curves		
Collins & Rigler (1982)	$\tau_{cr} = 1.24 w_s^{0.33}$	discarded
Critical shear velocity curves		
Komar & Clemens (1986) after Collins & Rigler (1982)	$u_{*,cr} = 0.482 (Rg\nu)^{0.282} w_s^{0.154}$	Fig. 9

After these considerations, the remaining 10 equations were all very similar (Figure 9). The largest differences occur in the cohesive regime. One equation deviates significantly from the other equations, which is the equation from Simões (2014). In the main part of the paper we used Zanke (2003), because this equation is physics-based, while many other equations are empirical fits to flume data, which could contain hidden gravity components in the coefficients. In addition, this equation has the advantage that it is valid for all grain sizes, while the empirical fits are only valid for a specific grain size range.

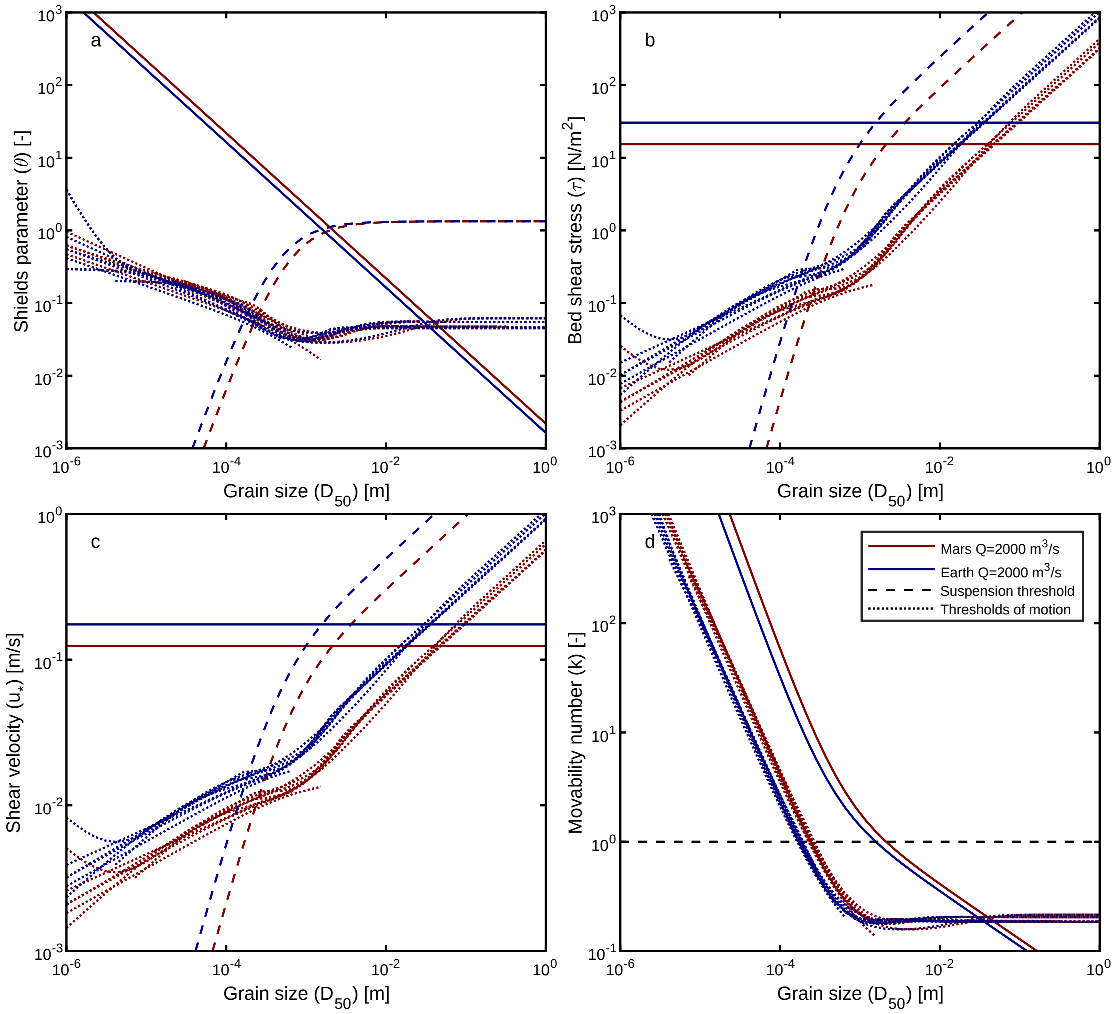

Figure 9: Mobility and suspension thresholds for (a) Shields parameter, i.e. nondimensional shear stress θ $[-]$, (b) bed shear stress τ $[N/m^2]$, (c) shear velocity u_* $[m/s]$ and (d) movability number k $[-]$ as a function of grain size for a given discharge Q $[m^3/s]$ and two gravities g of 3.7 and 9.8 m/s^2.

A.2 Fluvial sediment transport for a given water depth

In contrast to the results discussed in the main body of the paper, the following fluvial sediment transport results are based on a given water depth rather than a given water discharge. Meaning that the water depth between the Earth and Mars scenario is the same and no longer gravity dependent. We have already seem from Figure 8 that therefore the hydraulic radius and the Froude number are not gravity dependent. In addition the relation between shear stress and gravity is in this case a simple linear relation. Consequently the sediment transport parameters and fluxes differ as well. The non-dimensional shear stress is no longer depended on gravity, meaning that for the same water depth, Mars and Earth can transport the same grain sizes (Fig. 10b and c). For the suspension threshold there is a difference, but it is very minor. The movability number and the advection length only show higher numbers for Mars for smaller grain sizes. The effect of gravity on movability and advection length does not exist for coarse grains for a given water depth. Again this stresses that grain sizes are affected differently by gravity.

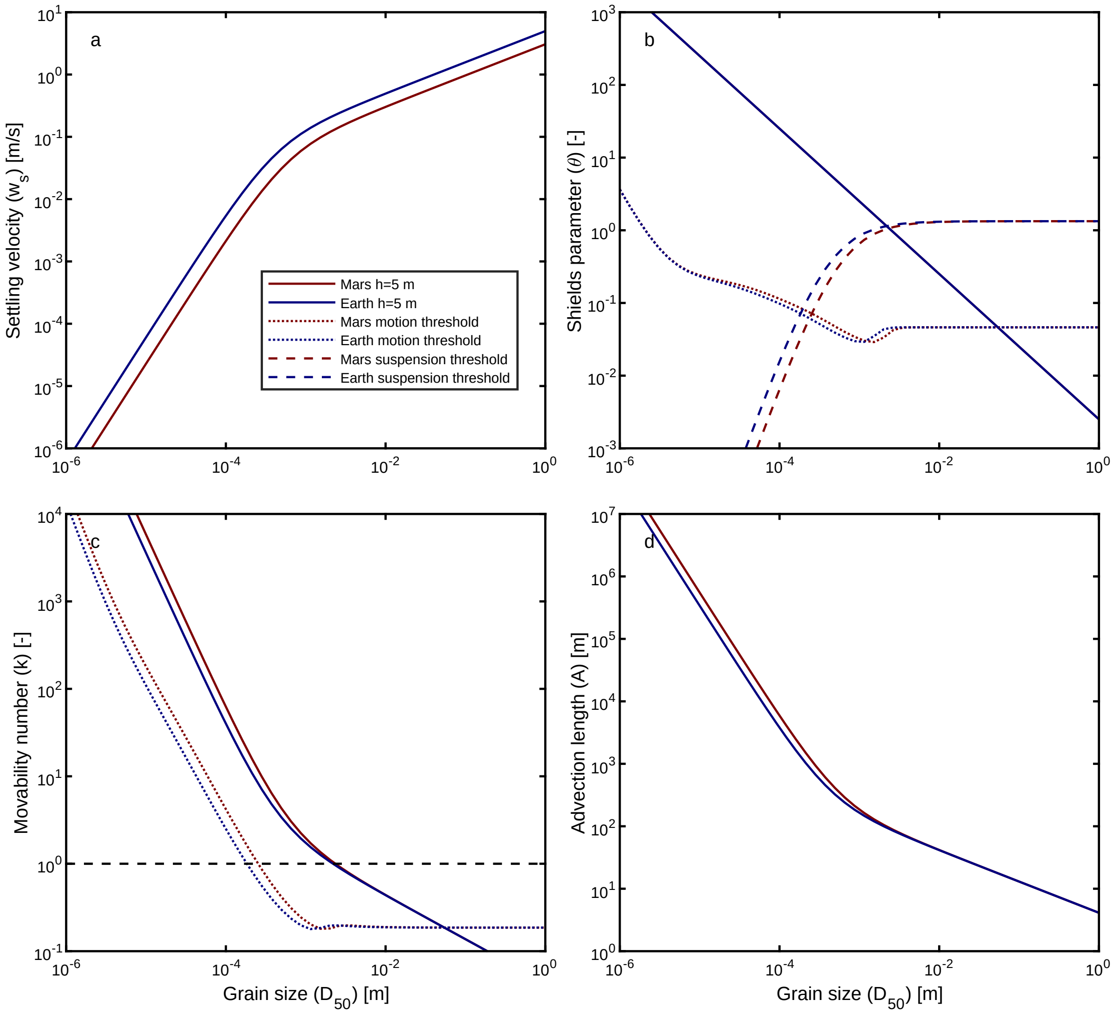

Figure 10: Fluvial sediment transport parameters (a) settling velocity w_s $[m/s]$, (b) Shields parameter θ $[-]$, (c) movability number k $[-]$, (d) advection length A $[m]$ as a function of grain size D_50 $[m]$ for Mars (red) and Earth (blue) gravity acceleration g $[m/s^2]$ and a given water depth h $[m]$. Please note the logarithmic scale in all subplots.

For a given water depth there is more bed load transport on Earth compared to Mars (Fig 11a). The effect of gravity on suspended load is more complicated (Fig 11b). The suspended transport predictors do not all show the same relation. A general trend can be extracted. For median grain sizes (sands), the suspended transport on Mars is a bit higher, while for very fine grain sizes (clay/silt), most equations predict that transport on Earth is slightly higher or equal. The effect on the coarse grain sizes (gravel/cobbles/boulders) is less important, because those are dominated by bed load transport. In total will still see that more sediment is transported in suspension on Mars for a given water depth (Fig 11d), similar as for a given discharge (Fig 5d). This mostly impacts the grain sizes at the bed-suspended load boundary. However, looking at the Mars/Earth total transport ratio, it is clear that in general (fine and coarse grains) the transport on Mars is lower for a giver water depth (Fig 11e). Nonetheless, the sands are still transported more efficiently on Mars. The net effect on transport will therefore depend on the sediment composition of the bed.

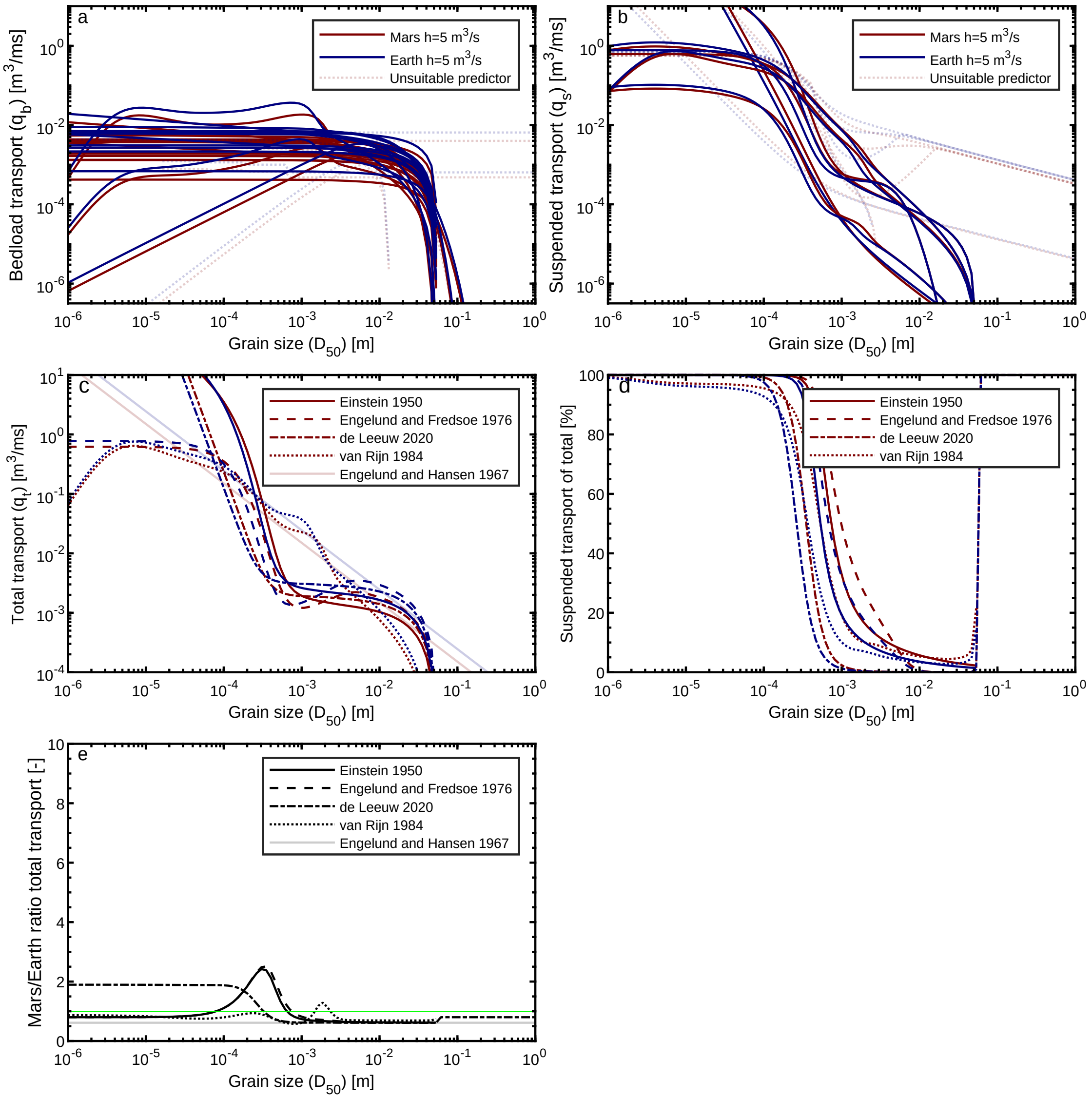

Figure 11: Fluvial transport rates for individual grain sizes. (a) Bed load transport q_b $[m^3/ms]$, (b) suspended transport q_s $[m^3/ms]$, (c) total transport q_t $[m^3/ms]$, (d) percentage of suspended transport of the total transport [%], (e) total transport ratio of Mars and Earth $[-]$ for Mars (red) and Earth (blue) gravity acceleration g $[m/s^2]$ and a given water depth h $[m]$.

Open Research

No data was used in this paper. The analytical model and visualisation scripts are available via GitHub: https://github.com/LBraat/Planetary-fluvial-sediment-transport-model-.git. For this analysis, Matlab version R2022b was used.

acknowledgments

This research was funded by a Rubicon fellowship (019.192EN.009) from the Dutch Research Council (NWO) and a Research Fellowship from the European Space Agency (ESA) awarded to Lisanne Braat. Reviewers will be acknowledged.

References

Akiyama, J. (1986). Entrainment of non cohesive sediment into suspension. In *Proc. 3rd int. symp. on river sedimentation, 1986* (pp. 804–813).

Amy, L., & Dorrell, R. (2021). Equilibrium sediment transport, grade and discharge for suspended-load-dominated flows on Earth, Mars and Titan. *Icarus*, *360*(15), 114243. doi: 10.1016/j.icarus.2020.114243

Ashida, K., & Michiue, M. (1972). Study on hydraulic resistance and bed-load transport rate in alluvial streams. In *Proceedings of the japan society of civil engineers* (Vol. 1972, pp. 59–69).

Baar, A., Boechat Albernaz, M., Van Dijk, W., & Kleinhans, M. (2019). Critical dependence of morphodynamic models of fluvial and tidal systems on empirical downslope sediment transport. *Nature communications*, *10*(1), 1–12.

Bagnold, R. A. (1962). Auto-suspension of transported sediment; turbidity currents. *Proceedings of the Royal Society of London. Series A. Mathematical and Physical Sciences*, *265*(1322), 315-319. doi: 10.1098/rspa.1962.0012

Bagnold, R. A. (1966). *An approach to the sediment transport problem from general physics.* US government printing office.

Bahia, R. S., Covey-Crump, S., Jones, M. A., & Mitchell, N. (2022). Discordance analysis on a high-resolution valley network map of mars: Assessing the effects of scale on the conformity of valley orientation and surface slope direction. *Icarus*, *383*, 115041. doi: 10.1016/j.icarus.2022.115041

Baker, V. R., & Milton, D. J. (1974). Erosion by catastrophic floods on Mars and Earth. *Icarus*, *23*(1), 27-41. doi: 10.1016/0019-1035(74)90101-8

Beheshti, A. A., & Ataie-Ashtiani, B. (2008). Analysis of threshold and incipient conditions for sediment movement. *Coastal Engineering*, *55*(5), 423-430. doi: 10.1016/j.coastaleng.2008.01.003

Birch, S., Hayes, A., Howard, A., Moore, J., & Radebaugh, J. (2016). Alluvial fan morphology, distribution and formation on titan. *Icarus*, *270*, 238–247. doi: 10.1016/j.icarus.2016.02.013

Braat, L., Kessel, T. V., Leuven, J. R., & Kleinhans, M. G. (2017). Effects of mud supply on large-scale estuary morphology and development over centuries to millennia. *Earth Surface Dynamics*, *5*(4), 617-652. doi: 10.5194/esurf-5-617-2017

Brown, R. H., Baines, K. H., Bellucci, G., Bibring, J.-P., Buratti, B. J., Capaccioni, F., ... others (2004). The cassini visual and infrared mapping spectrometer (vims) investigation. *Space Science Reviews*, *115*(1), 111–168. doi: 10.1007/S11214-004-1453-X

Brownlie, W. R. (1981). *Prediction of flow depth and sediment discharge in open channels* (Tech. Rep.). Californa Institute of Technology. doi: 10.7907/Z9KP803R

Burr, D. M., Emery, J. P., Lorenz, R. D., Collins, G. C., & Carling, P. A. (2006). Sediment transport by liquid surficial flow: Application to Titan. *Icarus*, *181*(1), 235–242. doi: 10.1016/j.icarus.2005.11.012

Burr, D. M., Taylor Perron, J., Lamb, M. P., Irwin III, R. P., Collins, G. C., Howard, A. D., ... others (2013). Fluvial features on titan: Insights from morphology and modeling. *Bulletin*, *125*(3-4), 299–321. doi: 10.1130/B30612.1

Cabrol, N. A., & Grin, E. A. (1999). Distribution, classification, and ages of Martian impact crater lakes. *Icarus*, *142*(1), 160–172. doi: 10.1006/icar.1999.6191

Cabrol, N. A., & Grin, E. A. (2001). The evolution of lacustrine environments on Mars: Is Mars only hydrologically dormant? *Icarus*, *149*(2), 291–328. doi: 10.1006/icar.2000.6530

Cabrol, N. A., & Grin, E. A. (2003). Overview on the formation of paleolakes and ponds on Mars. *Global and Planetary Change*, *35*(3-4), 199–219. doi: 10.1016/S0921-8181(02)00127-3

Camenen, B., & Larson, M. (2005). A general formula for non-cohesive bed load sediment transport. *Estuarine, Coastal and Shelf Science*, *63*(1-2), 249-260. doi: 10.1016/j.ecss.2004.10.019

Cao, Z., Pender, G., & Meng, J. (2006). Explicit formulation of the shields diagram for incipient motion of sediment. *Journal of Hydraulic Engineering*, *132*(10), 1097-1099. doi: 10.1061/(asce)0733-9429(2006)132:10(1097)

Carr, M. H. (2012). The fluvial history of Mars. *Philosophical Transactions of the Royal Society A: Mathematical, Physical and Engineering Sciences*, *370*(1966), 2193-2215. doi: 10.1098/rsta.2011.0500

Carrillo, V., Petrie, J., Timbe, L., Pacheco, E., Astudillo, W., Padilla, C., & Cisneros, F. (2021). Validation of an experimental procedure to determine bedload transport rates in steep channels with coarse sediment. *Water*, *13*(5), 672.

Celik, I., & Rodi, W. (1984). *A deposition-entrainment model for suspended sediment transport. report no* (Tech. Rep. No. Report No SFB 210/T/6). West-Germany: University of Karlsruhe.

Cheng, N.-S. (2002). Exponential formula for bedload transport. *Journal of Hydraulic Engineering*, *128*, 942-946. doi: 10.1061/(asce)0733-9429(2002)128:10(942)

Collins, M. B., & Rigler, J. K. (1982). The use of settling velocity in defining the initiation of motion of heavy mineral grains, under unidirectional flow. *Sedimentology*, *29*(3), 419-426. doi: 10.1111/j.1365-3091.1982.tb01804.x

De Toffoli, B., Plesa, A. C., Hauber, E., & Breuer, D. (2021). Delta deposits on Mars: A global perspective. *Geophysical Research Letters*, *48*(17), e2021GL094271. doi: 10.1029/2021GL094271

de Leeuw, J., Lamb, M. P., Parker, G., Moodie, A. J., Haught, D., Venditti, J. G., & Nittrouer, J. A. (2020). Entrainment and suspension of sand and gravel. *Earth Surface Dynamics*, *8*(2), 485-504. doi: 10.5194/esurf-8-485-2020

Di Achille, G., & Hynek, B. M. (2010). Ancient ocean on Mars supported by global distribution of deltas and valleys. *Nature Geoscience*, *3*(7), 459–463. doi: 10.1038/ngeo891

Dickson, J. L., Lamb, M. P., Williams, R. M. E., Hayden, A. T., & Fischer, W. W. (2021). The global distribution of depositional rivers on early Mars. *Geology*, *49*(5), 504–509. doi: 10.1130/g48457.1

Edmonds, D. A., & Slingerland, R. L. (2010). Significant effect of sediment cohesion on deltamorphology. *Nature Geoscience*, *3*(2), 105-109. doi: 10.1038/ngeo730

Einstein, H. A. (1942). Formulas for the transportation of bed load. *Transactions of the American Society of civil Engineers*, *107*(1), 561–577. doi: 10.1061/TACEAT.0005468

Einstein, H. A. (1950). *The bed-load function for sediment transportation in open channel flows* (No. 1026). US Department of Agriculture.

Engelund, F., & Fredsoe, J. (1976). A sediment transport model for straight alluvial channels. *Nordic Hydrology*, *7*(5), 293-306. doi: 10.2166/nh.1976.0019

Engelund, F., & Hansen, E. (1967). *A monograph on sediment transport in alluvial streams* (Tech. Rep.). Copenhagen: Technical University of Denmark.

Fairén, A. G. (2010). A cold and wet mars. *Icarus*, *208*(1), 165–175. doi: 10.1016/j.icarus.2010.01.006

Fassett, C. I., & Head III, J. W. (2008). Valley network-fed, open-basin lakes on Mars: Distribution and implications for Noachian surface and subsurface hydrology. *Icarus*, *198*(1), 37–56. doi: 10.1016/j.icarus.2008.06.016

Ferdowsi, B., Ortiz, C. P., Houssais, M., & Jerolmack, D. J. (2017). River-bed armouring as a granular segregation phenomenon. *Nature communications*, *8*(1), 1–10.

Ferguson, R. I., & Church, M. (2004). A simple universal equation for grain settling velocity. *Journal of Sedimentary Research*, *74*(6), 933–937. doi: 10.1306/051204740933

Francis, J. R. D. (1973). Experiments on the motion of solitary grains along the bed of a water-stream. In *Proceedings of the royal society of london. series a, mathematical and physical sciences* (Vol. 332, pp. 443–471). Royal Society of London.

Garcia, M. (1991). Entrainment of bed sediment into suspension. *Journal of Hydraulic Engineering*, *117*(4), 414-435.

Ghail, R. C., Hall, D., Mason, P. J., Herrick, R. R., Carter, L. M., & Williams, E. (2018). Vensar on envision: Taking earth observation radar to venus. *International journal of applied earth observation and geoinformation*, *64*, 365–376. doi: 10.1016/J.JAG.2017.02.008

Grotzinger, J. P., Gupta, S., Malin, M. C., Rubin, D. M., Schieber, J., Siebach, K., ... Wilson, S. A. (2015). Deposition, exhumation, and paleoclimate of an ancient lake deposit, Gale crater, Mars. *Science*, *350*(6257), aac7575. doi: 10.1126/science.aac7575

Grotzinger, J. P., Hayes, A. G., Lamb, M. P., & McLennan, S. M. (2013). *Sedimentary processes on earth, mars, titan, and venus.* University of Arizona Press. doi: 10.2458/azu_uapress_9780816530595-ch18

Harrison, K. P., & Grimm, R. E. (2008). Multiple flooding events in martian outflow channels. *Journal of Geophysical Research: Planets*, *113*(E02002). doi: 10.1029/2007JE002951

Hauber, E., Platz, T., Reiss, D., Le Deit, L., Kleinhans, M. G., Marra, W. A., ... Carbonneau, P. (2013). Asynchronous formation of Hesperian and Amazonian-aged deltas on Mars and implications for climate. *Journal of Geophysical Research E: Planets*, *118*(7), 1529–1544. doi: 10.1002/jgre.20107

Hayden, A. T., Lamb, M. P., Fischer, W. W., Ewing, R. C., McElroy, B. J., & Williams, R. M. (2019). Formation of sinuous ridges by inversion of river-channel belts in utah, usa, with implications for mars. *Icarus*, *332*, 92-110. doi: 10.1016/j.icarus.2019.04.019

Hunziker, R. P., & Jaeggi, M. N. R. (2002). Grain sorting processes. *Journal of Hydraulic Engineering*, *128*(12), 1060-1068. doi: 10.1061/ASCE0733-94292002128:121060

Hynek, B. M., Beach, M., & Hoke, M. R. T. (2010). Updated global map of Martian valley networks and implications for climate and hydrologic processes. *Journal of Geophysical Research*, *115*(E9), 1–14. doi: 10.1029/2009je003548

Hynek, B. M., & Phillips, R. J. (2003). New data reveal mature, integrated drainage systems on Mars indicative of past precipitation. *Geology*, *31*(9), 757–760. doi: 10.1130/G19607.1

Itakura, T., & Kishi, T. (1980). Open channel flow with suspended sediments. *Journal of the Hydraulics Division*, *106*(8), 1325–1343. doi: 10.1061/JYCEAJ.0005483

Khawja, S., Ernst, R., Samson, C., Byrne, P., Ghail, R., & MacLellan, L. (2020). Tesserae on venus may preserve evidence of fluvial erosion. *Nature communications*, *11*(1), 1–8. doi: 10.1038/s41467-020-19336-1

Kleinhans, M. G. (2005). Flow discharge and sediment transport models for estimating a minimum timescale of hydrological activity and channel and delta formation on Mars. *Journal of Geophysical Research: Planets*, *110*(12), 1-23. doi: 10.1029/2005JE002521

Kleinhans, M. G., Leuven, J. R., Braat, L., & Baar, A. (2017). Scour holes and ripples occur below the hydraulic smooth to rough transition of movable beds. *Sedimentology*, *64*(5), 1381-1401. doi: 10.1111/sed.12358

Kleinhans, M. G., Markies, H., Vet, S. J. D., Veld, A. C. I., & Postema, F. N. (2011). Static and dynamic angles of repose in loose granular materials under reduced gravity. *Journal of Geophysical Research: Planets*, *116*(11). doi: 10.1029/2011JE003865

Kleinhans, M. G., van de Kasteele, H. E., & Hauber, E. (2010). Palaeoflow reconstruction from fan delta morphology on Mars. *Earth and Planetary Science Letters*, *294*(3-4), 378–392. doi: 10.1016/j.epsl.2009.11.025

Komar, P. D. (1979). Comparisons of the hydraulics of water flows in Martian outflow channels with flows of similar scale on earth. *Icarus*, *37*(1), 156-181. doi: 10.1016/0019-1035(79)90123-4

Komar, P. D. (1980). Modes of sediment transport in channelized water flows with ramifications to the erosion of the Martian outflow channels. *Icarus*, *42*, 317–329. doi: 10.1016/0019-1035(80)90097-4

Komar, P. D., & Clemens, K. E. (1986). The relationship between a grain's settling velocity and threshold of motion under unidirectional currents. *Journal of Sedimentary Research*, *56*(2), 258-266. doi: 10.1306/212F88DC-2B24-11D7-8648000102C1865D

Konsoer, K. M., LeRoy, J., Burr, D., Parker, G., Jacobsen, R., & Turmel, D. (2018). Channel slope adjustment in reduced gravity environments and implications for martian channels. *Geology*, *46*(2), 183–186. doi: 10.1130/G39666.1

Kraal, E. R., Asphaug, E., Moore, J. M., Howard, A., & Bredt, A. (2008). Catalogue of large alluvial fans in martian impact craters. *Icarus*, *194*(1), 101–110. doi: 10.1016/j.icarus.2007.09.028

Lamb, M. P., Finnegan, N. J., Scheingross, J. S., & Sklar, L. S. (2015). New insights into the mechanics of fluvial bedrock erosion through flume experiments and theory. *Geomorphology*, *244*, 33–55.

Lamb, M. P., Grotzinger, J. P., Southard, J. B., & Tosca, N. J. (2012). Were aqueous ripples on mars formed by flowing brines? In *Sedimentary geology of mars* (p. 139-150). SEPM Special Publication No. 102. doi: 10.2110/pec.12.102.0139

Lapôtre, M. G. A., & Ielpi, A. (2020). The pace of fluvial meanders on mars and implications for the western delta deposits of jezero crater. *AGU Advances*, *1*(2). doi: 10.1029/2019av000141

Ledden, M. V., Kesteren, W. G. V., & Winterwerp, J. C. (2004). A conceptual framework for the erosion behaviour of sand-mud mixtures. *Continental Shelf Research*, *24*(1), 1-11. doi: 10.1016/j.csr.2003.09.002

Luque, R. F., & van Beek, R. (1976). Erosion and transport of bed-loadsediment. *Journal of Hydraulic Research*, *14*(2), 127-144. doi: 10.1080/00221687609499677

Mangold, N., Gupta, S., Gasnault, O., Dromart, G., Tarnas, J. D., Sholes, S. F., … Williford, K. H. (2021). Perseverance rover reveals an ancient delta-lake system and flood deposits at Jezero crater, Mars. *Science*, *374*(6568), 711-717. doi: 10.1126/science.abl4051

Mantz, P. A. (1977). Incipient transport of fine grains and flakes by fluids—extended Shields diagram. *Journal of the Hydraulics division*, *103*(6), 601–615. doi: 10.1061/JYCEAJ.0004766

McLean, S. R. (1992). On the calculation of suspended load for noncohesive sediments. *Journal of Geophysical Research*, *97*(C4), 5759-5770. doi: 10.1029/91JC02933

Meyer-Peter, E., & Müller, R. (1948). Formulas for bed-load transport. In *Iahsr 2nd meeting, stockholm, appendix 2.*

Meyer-Peter, E., & Müller, R. (1949). A formula for the calculation of bedload transport. *Schweizerische Bauzeitung*, *67*(3).

Miedema, S. A. (2010). Constructing the shields curve, a new theoretical approach and its applications..

Moore, J. M., & Howard, A. D. (2005). Large alluvial fans on Mars. *Journal of Geophysical Research E: Planets*, *110*(4), 1–24. doi: 10.1029/2004JE002352

Nicholas, A. (2013). Morphodynamic diversity of the world's largest rivers. *Geology*, *41*(4), 475-478. doi: 10.1130/G34016.1

Nielsen, P. (1992). *Coastal bottom boundary layers and sediment transport* (Vol. 4). World scientific.

Nixon, C., Lorenz, R., Achterberg, R., Buch, A., Coll, P., Clark, R., … others (2018). Titan's cold case files-outstanding questions after cassini-huygens. *Planetary and Space Science*, *155*, 50–72. doi: 10.1016/j.pss.2018.02.009

Paphitis, D. (2001). Sediment movement under unidirectional flows: an assessment of empirical threshold curves. *Coastal Engineering*, *43*(3-4), 227-245. doi: 10.1016/S0378-3839(01)00015-1

Parker, G. (1979). Hydraulic geometry of active gravel rivers. *Journal of the Hydraulics Division*, *105*(9), 1185–1201. doi: 10.1061/JYCEAJ.0005275

Peakall, J., Ashworth, P. J., & Best, J. L. (2007). Meander-bend evolution, alluvial architecture, and the role of cohesion in sinuous river channels: A flume study. *Journal of Sedimentary Research*, *77*(3-4), 197-212. doi: 10.2110/jsr.2007.017

Piliouras, A., Lauzon, R., & Rowland, J. C. (2021). Unraveling the combined effects of ice and permafrost on arctic delta morphodynamics. *Journal of Geophysical Research: Earth Surface*, *126*(4). doi: 10.1029/2020JF005706

Porco, C. C., West, R. A., Squyres, S., McEwen, A., Thomas, P., Murray, C. D., ... others (2004). Cassini imaging science: Instrument characteristics and anticipated scientific investigations at saturn. *Space Science Reviews*, *115*(1), 363–497. doi: 10.1007/S11214-004-1456-7

Ribberink, J. S. (1998). Bed-load transport for steady flows and unsteady oscillatory flows. *Coastal Engineering*, *34*(1-2), 59-82. doi: 10.1016/S0378-3839(98)00013-1

Righetti, M., & Lucarelli, C. (2007). May the Shields theory be extended to cohesive and adhesive benthic sediments? *Journal of Geophysical Research: Oceans*, *112*(5). doi: 10.1029/2006JC003669

Rijn, L. C. V. (1984a). Sediment transport, part I: Bed load transport. *Journal of Hydraulic Engineering*, *110*(10), 1431-1456.

Rijn, L. C. V. (1984b). Sediment transport, part II: Suspended load transport. *Journal of Hydraulic Engineering*, *110*(11), 1613-1641.

Rijn, L. C. V. (2007). Unified view of sediment transport by currents and waves. i: Initiation of motion, bed roughness, and bed-load transport. *Journal of Hydraulic Engineering*, *133*(6), 649-667. doi: 10.1061/(ASCE)0733-9429(2007)133:6(649)

Salese, F., Kleinhans, M. G., Mangold, N., Ansan, V., McMahon, W. J., de Haas, T., & Dromart, G. (2020). Estimated minimum life span of the Jezero fluvial delta (Mars). *Astrobiology*, *20*(8), 977–993. doi: 10.1089/ast.2020.2228

Schmeeckle, M. W. (2014). Numerical simulation of turbulence and sediment transport of medium sand. *Journal of Geophysical Research: Earth Surface*, *119*(6), 1240–1262. doi: 10.1002/2013JF002911

Schumm, S. A., & Stevens, M. A. (1973). Abrasion in place: a mechanism for rounding and size reduction of coarse sediments in rivers. *Geology*, *1*(1), 37–40. doi: 10.1130/0091-7613(1973)1⟨37:AIPAMF⟩2.0.CO;2

Sharp, R. P. (1973). Mars: Fretted and chaotic terrains. *Journal of Geophysical Research*, *78*(20), 4073-4083. doi: 10.1029/jb078i020p04073

Simões, F. J. (2014). Shear velocity criterion for incipient motion of sediment. *Water Science and Engineering*, *7*(2), 183-193. doi: 10.3882/j.issn.1674-2370.2014.02.006

Smart, G. M. (1984). Sediment transport formula for steep channels. *Journal of Hydraulic Engineering*, *110*, 267-176. doi: 10.1061/(ASCE)0733-9429(1984)110:3(267)

Smith, J. D., & McLean, S. R. (1977). Spatially averaged flow over a wavy surface. *Journal of Geophysical Research*, *82*(12), 1735-1746. doi: 10.1029/JC082i012p01735

Soulsby, R. L. (1997). Dynamics of marine sands: A manual for practical applications. *Oceanographic Literature Review*, *44*(9), 947.

Soulsby, R. L., & Damgaard, J. S. (2005). Bedload sediment transport in coastal waters. *Coastal Engineering*, *52*(8), 673-689. doi: 10.1016/j.coastaleng.2005.04.003

Soulsby, R. L., & Whitehouse, R. J. S. (1997). Threshold of sediment motion in coastal environments. In *Pacific coasts and ports'97. proceedings* (Vol. 1, pp. 149–154).

Vago, J. L., Westall, F., Coates, A. J., Jaumann, R., Korablev, O., Ciarletti, V., ... Carreau, C. (2017). Habitability on early mars and the search for biosignatures with the exomars rover. *Astrobiology*, *17*(6-7), 471-510. doi: 10.1089/ast.2016.1533 van der Vegt, H., Storms, J. E., Walstra, D. J., & Howes, N. C. (2016). Can bed load transport drive varying depositional behaviour in river delta environments? *Sedimentary Geology*, *345*, 19-32. doi: 10.1016/j.sedgeo.2016.08.009

Wall, S., Hayes, A., Bristow, C., Lorenz, R., Stofan, E., Lunine, J., … others (2010). Active shoreline of ontario lacus, titan: A morphological study of the lake and its surroundings. *Geophysical Research Letters*, *37*(5). doi: 10.1029/2009GL041821

Wilson, K. C. (1966). Bed-load transport at high shear stress. *Journal of the hydraulics division*, *92*(6), 49–59. doi: 10.1061/JYCEAJ.0001562

Wilson, S. A., Morgan, A. M., Howard, A. D., & Grant, J. A. (2021). The global distribution of craters with alluvial fans and deltas on Mars. *Geophysical Research Letters*, *48*(4), e2020GL091653. doi: 10.1029/2020GL091653

Witek, P. P., & Czechowski, L. (2015). Dynamical modelling of river deltas on titan and earth. *Planetary and Space Science*, *105*, 65–79. doi: 10.1016/j.pss.2014.11.005

Wong, M., & Parker, G. (2006). Reanalysis and correction of bed-load relation of Meyer-Peter and Müller using their own database. *Journal of Hydraulic Engineering*, *132*(11), 1159-1168. doi: 10.1061/ASCE0733-94292006132:111159

Wordsworth, R. D. (2016). The climate of early mars. *Annual Review of Earth and Planetary Sciences*, *44*, 381–408. doi: 10.1146/annurev-earth-060115-012355

Wright, S., Parker, G., & Asce, M. (2004). Flow resistance and suspended load in sand-bed rivers: Simplified stratification model. *Journal of Hydraulic Engineering*, *130*(8), 796-805. doi: 10.1061/(ASCE)0733-9429(2004)130:8(796)

Zanke, U. C. E. (2003). On the influence of turbulence on the initiation of sediment motion. *International Journal of Sediment Research*, *18*(1), 17–31. doi: 10.1016/0029-8018(79)90021-0